J. Mech. Phys. Solids 98 (2017) 390–410

Contents lists available at ScienceDirect

Journal of the Mechanics and Physics of Solids

journal homepage: www.elsevier.com/locate/jmps

Elastic wave propagation in finitely deformed layered materials

Pavel I. Galich[a], Nicholas X. Fang[b], Mary C. Boyce[c], Stephan Rudykh[a,*]

[a] Department of Aerospace Engineering, Technion – Israel Institute of Technology, Haifa 32000, Israel
[b] Department of Mechanical Engineering, Massachusetts Institute of Technology, Cambridge 02139-4307, MA, USA
[c] School of Engineering and Applied Science, Columbia University, New York 10027, USA

ARTICLE INFO

Keywords:
Layered materials
Elastic waves
Finite deformations
Band gaps
Phononic crystals

ABSTRACT

We analyze elastic wave propagation in highly deformable layered media with isotropic hyperelastic phases. Band gap structures are calculated for the periodic laminates undergoing large deformations. Compact explicit expressions for the phase and group velocities are derived for the long waves propagating in the finitely deformed composites. Elastic wave characteristics and band gaps are shown to be highly tunable by deformation. The influence of deformation on shear and pressure wave band gaps for materials with various composition and constituent properties are studied, finding advantageous compositions for producing highly tunable complete band gaps in low-frequency ranges. The shear wave band gaps are influenced through the deformation induced changes in effective material properties, whereas pressure wave band gaps are mostly influenced by deformation induced geometry changes. The wide shear wave band gaps are found in the laminates with small volume fractions of a soft phase embedded in a stiffer material; pressure wave band gaps of the low-frequency range appear in the laminates with thin highly compressible layers embedded in a nearly incompressible phase. Thus, by constructing composites with a small amount of a highly compressible phase, wide complete band gaps at the low-frequency range can be achieved; furthermore, these band gaps are shown to be highly tunable by deformation.

1. Introduction

Metamaterials have attracted considerable attention due to their unusual properties such as negative elastic moduli (Babaee et al., 2013), mass density (Brunet et al., 2013), and negative refractive index (Liu et al., 2011). *Soft* metamaterials, capable of large deformations, open promising opportunities for tuning and switching acoustic properties by deformation (Bertoldi and Boyce, 2008a; Rudykh and Boyce, 2014b; Babaee et al., 2016). Even relatively simple deformable homogeneous materials can exhibit switchable acoustic functionalities upon applied deformations (Galich and Rudykh, 2015a). Indeed, soft *microstructured* metamaterials possess even greater capability for transforming and tuning wave propagation by external stimuli, such as mechanical loading (Rudykh and Boyce, 2014b; Bertoldi and Boyce, 2008b), electric (Gei et al., 2011; Galich and Rudykh, 2016) or magnetic fields (Destrade and Ogden, 2011). Applied deformation can lead to a change in the internal geometry of a phononic crystal giving rise to formation and/or transformation of phononic band gaps (BGs) (Kushwaha et al., 1993, 1994; Tanaka et al., 2000; Hussein, 2009). Moreover, local material properties can also change as a result of inhomogeneous distribution of local deformation fields leading to local softening or stiffening (Galich and Rudykh, 2015b). In fact, these effects are of significant importance for understanding elastic wave phenomena in soft biological tissues that are frequently found in a deformed state due to growth or other

* Corresponding author.
E-mail address: rudykh@technion.ac.il (S. Rudykh).

http://dx.doi.org/10.1016/j.jmps.2016.10.002
Received 4 July 2016; Received in revised form 27 September 2016; Accepted 6 October 2016
Available online 11 October 2016
0022-5096/

biological processes. Large deformations together with material heterogeneity may give rise to elastic instabilities (Bertoldi et al., 2008; Rudykh and deBotton, 2012; Li et al., 2013; Slesarenko and Rudykh, 2016) – a phenomenon actively used in material design by nature (Crosby, 2010). Recently, this approach has been employed to utilize instability-induced dramatic microstructure transformations and achieve remarkable tunability of acoustic metamaterials (Bertoldi and Boyce, 2008a; Rudykh and Boyce, 2014b; Babaee et al., 2016). Inspired by possible applications – such as noise reducers, acoustic mirrors and filters, waveguides, to name a few – a number of recent works were dedicated to the analysis of influence of material parameters (Zhou et al., 2009), topologies (Mousanezhad et al., 2015), deformations (Bertoldi and Boyce, 2008a), and stiffening effects (Wang et al., 2013) on elastic wave propagation and band gap structure in various phononic crystals. Nevertheless, realization of the complex microstructures remains challenging, especially, at small length-scales desirable for some applications. Recent advances in additive and layer-by-layer material manufacturing allow fabrication of highly structured layered materials ranging from sub-light-wavelength scale (Kolle et al., 2013) to meso-length-scale (Li et al., 2013; Rudykh et al., 2015). These layered materials can produce complete phononic BGs – the frequency ranges where neither pressure nor shear waves can propagate – spanning different frequency ranges depending on the characteristic microstructure size. Moreover, these BGs can be further actively controlled by deformation. In this work, we specifically focus on identifying the key parameters defining the appearance of shear wave, pressure wave, and complete BGs in finitely deformed layered composites with isotropic phases. Special attention is given to the influence of deformation on the acoustic characteristics and BGs.

The layered media exhibit both geometrical and material non-linearities when subjected to finite strains; hence, these non-linear effects need to be taken into account in the model. To this end, we first obtain the solution for the finitely deformed state of hyperelastic periodic layered materials, and then perform the wave propagation analysis in terms of the incremental small amplitude motions *superimposed* on the finitely deformed state. By utilizing an exact analytical solution for the finitely deformed incompressible laminates with alternating isotropic hyperelastic phases, we derive explicit relations for the phase and group velocities in finitely deformed incompressible laminates in the long wave limit. Moreover, based on the expressions of the phase velocities for finitely deformed compressible homogeneous materials, we estimate the phase velocities of pressure and shear waves propagating perpendicular to the layers in finitely deformed laminates comprised of *compressible* phases. Next, considering steady-state plane waves in layered media, we thoroughly analyze band gap structures for shear and pressure waves propagating perpendicular to the layers in soft laminates with nearly incompressible and highly compressible phases. We show that wide shear wave BGs at the low-frequency range can be achieved by constructing laminates with thin soft layers embedded in a stiffer matrix. Moreover, these band gaps can be further tuned by deformation through the change in the geometry and effective properties of the phases. We find that for layers with pronounced stiffening effects (such as Gent materials), the change in the material effective properties prevails over the change in the geometry. However, for the materials with weak stiffening effects (such as neo-Hookean materials) the deformation induced change in the material properties is entirely compensated by the change in the geometry. We find that wide pressure wave BGs at the low-frequency range are attainable in laminates with small amount of highly compressible phase embedded in a nearly incompressible matrix. These pressure wave BGs are highly tunable by deformation. The laminate geometry change induced by deformation is shown to be the dominant factor influencing pressure wave BGs (as compared to the influence of the change in the effective material properties). Consequently, wide *complete* BGs at low-frequency range can be achieved by including a small amount of thin highly compressible phase into a nearly incompressible matrix. Furthermore, these complete BGs can be widened and shifted via deformation.

2. Theoretical background

Consider a continuum body and identify each point in the undeformed configuration with its position vector $\mathbf{X}$. When the body is deformed, the new location of a point is defined by mapping function $\mathbf{x} = \boldsymbol{\chi}(\mathbf{X}, t)$. Thus, the deformation gradient is $\mathbf{F} = \partial\mathbf{x}/\partial\mathbf{X}$, and its determinant $J \equiv \det\mathbf{F} > 0$. For a hyperelastic material whose constitutive behavior is described in terms of a strain energy function $\psi(\mathbf{F})$, the first Piola–Kirchhoff stress tensor is given by

$$\mathbf{P} = \frac{\partial\psi(\mathbf{F})}{\partial\mathbf{F}}. \tag{1}$$

The corresponding true or Cauchy stress tensor is related to the first Piola–Kirchhoff stress tensor via the relation $\boldsymbol{\sigma} = J^{-1}\mathbf{P}\mathbf{F}^T$. In the absence of body forces the equations of motion can be written in the undeformed configuration as

$$\mathrm{Div}\,\mathbf{P} = \rho_0 \frac{D^2\boldsymbol{\chi}}{Dt^2}, \tag{2}$$

where ρ_0 is the initial density of the material, and the $D^2(\bullet)/Dt^2$ operator represents the material time derivative. If the deformation is applied quasi-statically, the right hand part of Eq. (2) can be assumed to be zero, and the equilibrium equation is obtained, namely

$$\mathrm{Div}\,\mathbf{P} = 0. \tag{3}$$

2.1. Wave propagation in homogeneous media

Consider next small amplitude motions[1] superimposed on the equilibrium state. The equations of the incremental motions are

$$\text{Div}\,\mathbf{P} = \rho_0 \frac{D^2\mathbf{u}}{Dt^2}, \tag{4}$$

where $\dot{\mathbf{P}}$ is an incremental change in the first Piola–Kirchhoff stress tensor and $\mathbf{u}$ is the incremental displacement. The incremental change in the deformation gradient is $\dot{\mathbf{F}} = \text{Grad}\,\mathbf{u}$.

The linearized constitutive law can be written as

$$\dot{P}_{ij} = \mathcal{A}_{0ijkl}\dot{F}_{kl} \tag{5}$$

with the tensor of elastic moduli defined as $\mathcal{A}_{0i\alpha k\beta} = \partial^2\psi/\partial F_{i\alpha}\partial F_{k\beta}$. Under substitution of Eq. (5) into Eq. (4) the incremental motion equation takes the form of

$$\mathcal{A}_{0ijkl}u_{k,lj} = \rho_0 \frac{D^2u_i}{Dt^2}. \tag{6}$$

To analyze small amplitude motions superimposed on a finite deformation, we present (6) in the updated Lagrangian formulation

$$\mathcal{A}_{ijkl}u_{k,lj} = \rho\frac{\partial^2 u_i}{\partial t^2}, \tag{7}$$

where $\mathcal{A}_{iqkp} = J^{-1}\mathcal{A}_{0ijkl}F_{pl}F_{qj}$ and $\rho = J^{-1}\rho_0$ is the density of the deformed material.

We seek a solution for Eq. (7) in the form of the plane waves with constant polarization

$$\mathbf{u} = \mathbf{g}h(\mathbf{n}\cdot\mathbf{x} - ct), \tag{8}$$

where h is a twice continuously differentiable function and unit vector $\mathbf{g}$ is the polarization; the unit vector $\mathbf{n}$ defines the direction of propagation of the wave, and c is the phase velocity of the wave.

By substitution of (8) into (7), we obtain

$$\mathbf{Q}(\mathbf{n})\cdot\mathbf{g} = \rho c^2\mathbf{g}, \tag{9}$$

where

$$Q_{ij} = \mathcal{A}_{ijkl}n_j n_l \tag{10}$$

is the acoustic tensor which defines the condition of propagation of the infinitesimal plane waves.

For incompressible materials $J = 1$ and $\mathbf{g}\cdot\mathbf{n} = 0$, and Eq. (9) reads as

$$\widehat{\mathbf{Q}}(\mathbf{n})\cdot\mathbf{g} = \rho c^2\mathbf{g}, \tag{11}$$

where $\widehat{\mathbf{Q}} = \hat{\mathbf{I}}\cdot\mathbf{Q}\cdot\hat{\mathbf{I}}$ and $\hat{\mathbf{I}} = \mathbf{I} - \mathbf{n}\otimes\mathbf{n}$ is the projection on the plane normal to $\mathbf{n}$.

2.2. Wave propagation in periodic layered media

Consider periodic laminates constructed of two alternating phases with initial volume fractions v_a and $v_b = 1 - v_a$. Here and thereafter, the fields and parameters of the constituents are denoted by subscripts $(\bullet)_a$ and $(\bullet)_b$, respectively. Geometrically, the layers are characterized by their thicknesses $d_a^o = v_a d^o$ and $d_b^o = v_b d^o$, where d^o is the initial period of the laminate (see Fig. 1(a)).

When laminates are deformed (see Fig. 1(b)), the layer thicknesses change as follows:

$$d_a = \lambda_{1a}d_a^o, \quad d_b = \lambda_{1b}d_b^o, \quad \text{and} \quad d = \overline{\lambda}_1 d^o, \tag{12}$$

where $\overline{\lambda}_1 = v_a\lambda_{1a} + v_b\lambda_{1b}$; $\lambda_{1a,b}$ are the stretch ratios in the direction $\mathbf{e}_1$ for phases a and b, respectively.

Let us consider steady-state compression small amplitude plane waves superimposed on a finitely deformed state and propagating along the x direction orthogonal to the interface between the layers (Bedford and Drumheller, 1994) (see Fig. 1(b) and (c)). For each layer, the one-dimensional wave equation takes the form

$$\frac{\partial^2 u_\xi}{\partial t^2} = c_\xi^2\frac{\partial^2 u_\xi}{\partial x^2}, \tag{13}$$

where u_ξ denotes the displacement in x direction, and subscript ξ stands for a or b. We seek a solution within each layer in the following form[2]:

$$u_\xi = A_\xi e^{i(k_\xi x - \omega t)} + B_\xi e^{i(-k_\xi x - \omega t)}, \tag{14}$$

where ω denotes the angular frequency, and $k_\xi = \omega/c_\xi$ is the wave number. The normal stress within each layer is

[1] Note that we consider only small amplitude elastic waves (Ogden, 1997); the amplitudes of the superimposed on finite deformations displacements of the material points are assumed to be much (infinitesimally) smaller than any characteristic dimension of the composite, $|\mathbf{u}|/d \ll 1$; so that its geometry and the constitutive properties of the material (such as density and tangent elastic moduli) at each point of the composite are assumed to be unchanged by these small amplitude motions.

[2] Note that we consider only small amplitude elastic waves here, i.e. $u_\xi/d \ll 1$.

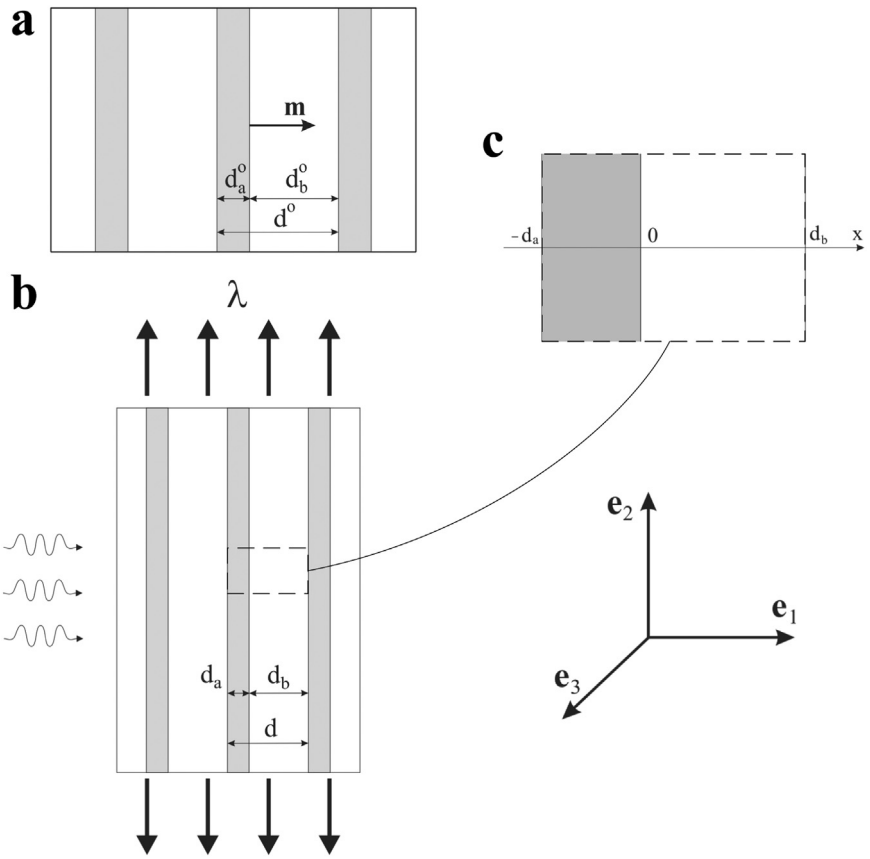

Fig. 1. Schematic representation of the undeformed (a) and deformed (b) periodic layered material with alternating phases a and b. A unit cell (c); ($\mathbf{e}_1$, $\mathbf{e}_2$, $\mathbf{e}_3$) is the orthonormal basis.

$$\sigma_\xi = \rho_\xi c_\xi^2 \frac{\partial u_\xi}{\partial x} = \frac{z_\xi^2}{\rho_\xi}\frac{\partial u_\xi}{\partial x}, \tag{15}$$

where $z_\xi = \rho_\xi c_\xi$ is the acoustic impedance.

The interface continuity condition between the layers implies

$$u_a(0,\, t) = u_b(0,\, t) \quad \text{and} \quad \sigma_a(0,\, t) = \sigma_b(0,\, t), \tag{16}$$

where we assign $x = 0$ to be the interface between the layers of the unit cell (Fig. 1(c)).

Two additional conditions are obtained from the periodicity of the material by the use of Floquet theorem. For this reason we adjust Eq. (14) to be the steady-state wave expression with the same wave number k for both materials

$$u_\xi = U_\xi(x) e^{i(kx-\omega t)}, \tag{17}$$

where

$$U_\xi(x) = A_\xi e^{iK_\xi^- x} + B_\xi e^{-iK_\xi^+ x} \quad \text{and} \quad K_\xi^\pm = k_\xi \pm k. \tag{18}$$

According to Floquet theorem, function $U_\xi(x)$ must be periodic functions of x with the period equal to the length of the unit cell, namely $d = d_a + d_b$,

$$U_a(-d_a) = U_b(d_b). \tag{19}$$

The corresponding relations for the stress are

$$\sigma_\xi = \Sigma_\xi(x) e^{i(kx-\omega t)}, \tag{20}$$

where

$$\Sigma_\xi(x) = i z_\xi \omega (A_\xi e^{iK_\xi^- x} - B_\xi e^{-iK_\xi^+ x}) \tag{21}$$

and

$$\Sigma_a(-d_a) = \Sigma_b(d_b). \tag{22}$$

Thus, Eqs. (16), (19) and (22) together with (17), (18), (20) and (21) yield the dispersion relation $\omega = \omega(k)$ for the steady-state wave (Rytov, 1956)

$$\cos kd = \cos\left(\frac{\omega d_a}{c_a}\right)\cos\left(\frac{\omega d_b}{c_b}\right) - \frac{1}{2}\left(\frac{z_a}{z_b} + \frac{z_b}{z_a}\right)\sin\left(\frac{\omega d_a}{c_a}\right)\sin\left(\frac{\omega d_b}{c_b}\right). \tag{23}$$

The dispersion relation (23) is derived for pressure waves. However, the same expression can be obtained for shear waves by considering displacements perpendicular to axis x in Eq. (13). In this case, the phase velocities of shear waves are used in (23) to obtain the dispersion relation for shear waves.

3. Results

The macroscopically applied loading is expressed in terms of the average deformation gradient

$$\overline{\mathbf{F}} = v_a\mathbf{F}_a + v_b\mathbf{F}_b, \tag{24}$$

where $\mathbf{F}_a$ and $\mathbf{F}_b$ are the corresponding deformation gradients within each phase. The displacement continuity condition along the interface between the layers yields the condition for $\mathbf{F}_a$ and $\mathbf{F}_b$

$$(\mathbf{F}_a - \mathbf{F}_b)\cdot\mathbf{q} = \mathbf{0} \tag{25}$$

and the interface stress jump condition is

$$(\mathbf{P}_a - \mathbf{P}_b)\cdot\mathbf{m} = \mathbf{0}, \tag{26}$$

where unit vector $\mathbf{m}$ denotes the initial lamination direction (see Fig. 1(a)), $\mathbf{q}$ is an arbitrary unit vector orthogonal to $\mathbf{m}$.

Loading paths. Although the analysis is general and can be applied for materials subjected to any deformation $\overline{\mathbf{F}}$, the examples are given for (i) in-plane and (ii) equibiaxial deformations. The corresponding macroscopic deformation gradients are

(i) *in-plane tension*

$$\overline{\mathbf{F}} = \overline{\lambda}_1\mathbf{e}_1 \otimes \mathbf{e}_1 + \lambda\mathbf{e}_2 \otimes \mathbf{e}_2 + \mathbf{e}_3 \otimes \mathbf{e}_3, \tag{27}$$

(ii) *equibiaxial deformation*

$$\overline{\mathbf{F}} = \overline{\lambda}_1\mathbf{e}_1 \otimes \mathbf{e}_1 + \lambda(\mathbf{I} - \mathbf{e}_1 \otimes \mathbf{e}_1), \tag{28}$$

where λ is the applied stretch in the direction of the layers (see Fig. 1), and $\overline{\lambda}_1$ is an unknown and needs to be calculated. For an incompressible laminate $\overline{\lambda}_1 = \lambda^{-1}$ and $\overline{\lambda}_1 = \lambda^{-2}$ for in-plane and equibiaxial deformations, respectively. To describe the behavior of *incompressible* phases, we utilize the neo-Hookean strain energy function (Ogden, 1997)

$$\psi_\xi^{inc} = \frac{\mu_\xi}{2}(\mathbf{F}_\xi\colon \mathbf{F}_\xi - 3), \tag{29}$$

where μ_ξ is the initial shear modulus.

The constitutive behavior of the *compressible* phases is assumed to be governed by the extended neo-Hookean strain energy function (Ogden, 1997)

$$\psi_\xi^{comp} = \frac{\mu_\xi}{2}(\mathbf{F}_\xi\colon \mathbf{F}_\xi - 3) - \mu_\xi \ln J_\xi + \frac{\Lambda_\xi}{2}(J_\xi - 1)^2, \tag{30}$$

where Λ_ξ is the first Lame's parameter. Recall that Λ relates to the bulk modulus as $K = \Lambda + 2\mu/3$.

By making use of strain energy function (30) together with (25) and (26), the unknown stretch ratios λ_{1a} and λ_{1b} are determined. In particular, the explicit expressions are

(i) *in-plane tension*

$$\lambda_{1a} = \frac{\eta_a\lambda\gamma + \sqrt{2(4 + \eta_a(4 + \eta_a)\lambda^2)(2 + \eta_b\lambda(\gamma + 2\lambda))}}{2(1 + \eta_a\lambda^2)\gamma} \quad \text{and} \quad \lambda_{1b} = \frac{\gamma}{2(1 + \eta_b\lambda^2)}, \tag{31}$$

where $\eta_a = \Lambda_a/\mu_a$, $\eta_b = \Lambda_b/\mu_b$, and $\gamma = \eta_b\lambda + \sqrt{4 + \eta_b(4 + \eta_b)\lambda^2}$;

(ii) *equibiaxial deformation*

$$\lambda_{1a} = \frac{\eta_a\lambda^2\zeta + \sqrt{2(4 + \eta_a(4 + \eta_a)\lambda^4)(2 + \eta_b\lambda^2(\zeta + 2\lambda^2))}}{2(1 + \eta_a\lambda^4)\zeta} \quad \text{and} \quad \lambda_{1b} = \frac{\zeta}{2(1 + \eta_b\lambda^4)}, \tag{32}$$

where $\zeta = \eta_b\lambda^2 + \sqrt{4 + \eta_b(4 + \eta_b)\lambda^4}$.

To account for the stiffening effects (for example, due to a finite extensibility of polymer chains) in finitely deformed incompressible laminates, we employ the strain-energy density function corresponding to an approximation of the Arruda–Boyce model (Arruda and Boyce, 1993), namely the Gent model (Gent, 1996)

$$\psi_{\xi}^{inc} = -\frac{\mu_{\xi} J_{m\xi}}{2} \ln\left(1 - \frac{\mathbf{F}_{\xi}\colon \mathbf{F}_{\xi} - 3}{J_{m\xi}}\right), \tag{33}$$

where $J_{m\xi}$ is the so-called dimensionless locking parameter defining the lock-up stretch ratio, such that in the limit $(\mathbf{F}_{\xi}\colon \mathbf{F}_{\xi} - 3) \to J_{m\xi}$, the strain energy becomes unbounded. Thus, for incompressible Gent materials under in-plane tension, the lock-up stretch ratios can be calculated as

$$\lambda_{\xi}^{lock} = (\sqrt{J_{m\xi} + 4} \pm \sqrt{J_{m\xi}})/2, \tag{34}$$

where "+" and "−" correspond to the extension ($\lambda > 1$) and contraction ($\lambda < 1$), respectively. Clearly, in the limit $J_m \to \infty$, the strain-energy function (33) reduces to the neo-Hookean material model (29).

The constitutive behavior of the *compressible* phases exhibiting strong stiffening is assumed to be governed by the extended Gent strain energy function (Horgan and Saccomandi, 2004; Wang et al., 2013)

$$\psi_{\xi}^{comp} = -\frac{\mu_{\xi} J_{m\xi}}{2} \ln\left(1 - \frac{\mathbf{F}_{\xi}\colon \mathbf{F}_{\xi} - 3}{J_{m\xi}}\right) - \mu_{\xi} \ln J_{\xi} + \left(\frac{\Lambda_{\xi}}{2} - \frac{\mu_{\xi}}{J_{m\xi}}\right)(J_{\xi} - 1)^2, \tag{35}$$

Again, in the limit $J_m \to \infty$, the strain-energy function (35) reduces to the extended neo-Hookean material model (30).

3.1. Long wave estimates for finitely deformed layered materials

3.1.1. Incompressible laminates

First, let us consider layered materials with *incompressible* phases. The incompressibility assumption allows us to obtain a closed form exact solution for finitely deformed periodic layered materials with neo-Hookean phases (deBotton, 2005; Tzianetopoulou, 2007; Rudykh and Boyce, 2014a; Spinelli and Lopez-Pamies, 2015). By utilizing the exact analytical solution, an effective strain energy function can be constructed (Spinelli and Lopez-Pamies, 2015)

$$\psi(\overline{\mathbf{F}}) = \frac{\overline{\mu}}{2}(\overline{\mathbf{F}}\colon \overline{\mathbf{F}} - 3) - \frac{\overline{\mu} - \breve{\mu}}{2}\left(\mathbf{m}\cdot\overline{\mathbf{C}}\cdot\mathbf{m} - \frac{1}{\mathbf{m}\cdot\overline{\mathbf{C}}^{-1}\cdot\mathbf{m}}\right), \tag{36}$$

where $\overline{\mathbf{C}} = \overline{\mathbf{F}}^{T}\cdot\overline{\mathbf{F}}$ is the average right Cauchy–Green deformation tensor, and

$$\overline{\mu} = v_a\mu_a + v_b\mu_b \quad \text{and} \quad \breve{\mu} = \left(\frac{v_a}{\mu_a} + \frac{v_b}{\mu_b}\right)^{-1}. \tag{37}$$

Note that while the solution for finitely deformed laminates is provided in deBotton (2005), Tzianetopoulou (2007), Rudykh and Boyce (2014a), Spinelli and Lopez-Pamies (2015), the strain energy function in the form of (36) is reported by Spinelli and Lopez-Pamies (2015).

The acoustic tensor (11) corresponding to the strain energy function (36), takes the form

$$\widehat{\mathbf{Q}}(\mathbf{n}, \overline{\mathbf{F}}) = q_1\hat{\mathbf{I}} + q_2(\hat{\mathbf{I}}\cdot\overline{\mathbf{F}}^{-T}\cdot\mathbf{m}) \otimes (\hat{\mathbf{I}}\cdot\overline{\mathbf{F}}^{-T}\cdot\mathbf{m}), \tag{38}$$

where

$$q_1 = \overline{\mu}(\mathbf{n}\cdot\overline{\mathbf{B}}\cdot\mathbf{n}) + (\breve{\mu} - \overline{\mu})(\mathbf{n}\cdot\overline{\mathbf{F}}\cdot\mathbf{m})^2 \quad \text{and} \quad q_2 = \frac{\overline{\mu} - \breve{\mu}}{\alpha^2}\left(\frac{4\beta^2}{\alpha} - 1\right), \tag{39}$$

where $\overline{\mathbf{B}} = \overline{\mathbf{F}}\cdot\overline{\mathbf{F}}^{T}$ is the average left Cauchy–Green deformation tensor, $\alpha = \mathbf{m}\cdot\overline{\mathbf{C}}^{-1}\cdot\mathbf{m}$, and $\beta = \mathbf{n}\cdot\overline{\mathbf{F}}^{-T}\cdot\mathbf{m}$. One can show that the acoustic tensor (38) has the following eigenvalues in the two-dimensional space normal to $\mathbf{n}$:

$$a_1 = q_1 \quad \text{and} \quad a_2 = q_1 + q_2(\alpha - \beta^2). \tag{40}$$

In general, we have two distinct shear waves propagating in the finitely deformed incompressible laminate. The corresponding phase velocities are

$$\overline{c}_{sw}^{(1)} = \sqrt{a_1/\overline{\rho}_0} \quad \text{and} \quad \overline{c}_{sw}^{(2)} = \sqrt{a_2/\overline{\rho}_0}, \tag{41}$$

where $\overline{\rho}_0 = v_a\rho_{0a} + v_b\rho_{0b}$ is the average initial density of the laminate.

Note that the phase velocities of shear waves (41) coincide only for special cases of applied deformation and direction of wave propagation. For instance, for wave propagating perpendicular to the layers, i.e. $\mathbf{n} = \mathbf{m} = \mathbf{e}_1$, the phase velocities of shear waves coincide:

(i) *in-plane tension*

$$\overline{c}_{sw} = \overline{c}_{sw}^{(1)} = \overline{c}_{sw}^{(2)} = \lambda^{-1}\sqrt{\breve{\mu}/\overline{\rho}_0}, \tag{42}$$

(ii) *equibiaxial deformation*

$$\overline{c}_{sw} = \overline{c}_{sw}^{(1)} = \overline{c}_{sw}^{(2)} = \lambda^{-2}\sqrt{\breve{\mu}/\overline{\rho}_0}. \tag{43}$$

However, if the wave propagates along the layers, i.e. $\mathbf{m} = \mathbf{e}_1$ and $\mathbf{n} = \mathbf{e}_2$, the phase velocities of shear waves are distinct:
(i) *in-plane tension*

$$\bar{c}_{sw}^{(1)} = \lambda\sqrt{\overline{\mu}/\overline{\rho}_0} \quad (\mathbf{g} = \mathbf{e}_3) \tag{44}$$

and

$$\bar{c}_{sw}^{(2)} = \lambda^{-1}\sqrt{(\check{\mu} + (\lambda^4 - 1)\overline{\mu})/\overline{\rho}_0} \quad (\mathbf{g} = \mathbf{e}_1), \tag{45}$$

(ii) *equibiaxial deformation*

$$\bar{c}_{sw}^{(1)} = \lambda\sqrt{\overline{\mu}/\overline{\rho}_0} \quad (\mathbf{g} = \mathbf{e}_3) \tag{46}$$

and

$$\bar{c}_{sw}^{(2)} = \lambda^{-2}\sqrt{(\check{\mu} + (\lambda^6 - 1)\overline{\mu})/\overline{\rho}_0} \quad (\mathbf{g} = \mathbf{e}_1). \tag{47}$$

Note that expressions (45) and (47) yield explicit expressions for the critical stretch ratios corresponding to the onset of macroscopic instability under in-plane and equibiaxial contractions:
(i) *in-plane tension*

$$\lambda_{cr}^{pt} = \left(1 - \frac{\check{\mu}}{\overline{\mu}}\right)^{1/4}, \tag{48}$$

(ii) *equibiaxial deformation*

$$\lambda_{cr}^{bt} = \left(1 - \frac{\check{\mu}}{\overline{\mu}}\right)^{1/6}. \tag{49}$$

It is worth mentioning that Eq. (48) agrees with the results obtained by Rosen (1965), and Triantafyllidis and Maker (1985) utilizing distinct approaches.

To illustrate the influence of the deformation and direction of wave propagation on the elastic waves in the layered materials, we construct slowness curves (which are commonly used in acoustics, Auld, 1990) by the use of the explicit relations (41). Fig. 2 shows examples of the slowness curves $\bar{s}_{sw}(\varphi) = 1/\bar{c}_{sw}(\varphi)$ for (a) out-of-plane (with polarization $\mathbf{e}_3$) and (b) in-plane (with polarization lying in plane $\mathbf{e}_1 - \mathbf{e}_2$) shear waves in layered material undergoing equibiaxial deformation, where the direction of propagation is defined as $\mathbf{n} = (\cos\varphi, \sin\varphi, 0)$. Note that the critical stretch ratio for the laminate with $\nu_a = 0.1$ and $\mu_a/\mu_b = 20$ undergoing equibiaxial contraction is $\lambda_{cr}^{bt} = 0.92$; therefore, we present slowness curves corresponding to the equibiaxially contracted laminate ($\lambda = 0.95$) in the macroscopically stable state. The slowness curves clearly indicate the significant influence of the applied deformation on the wave propagation. Specifically, an extension results in a decrease of the phase velocities of the shear waves propagating perpendicular to the layers; while the phase velocities increase for waves propagating along the layers since these directions experience extension. The phase velocity of the in-plane shear wave in the equibiaxially deformed laminate has maxima for certain directions of wave

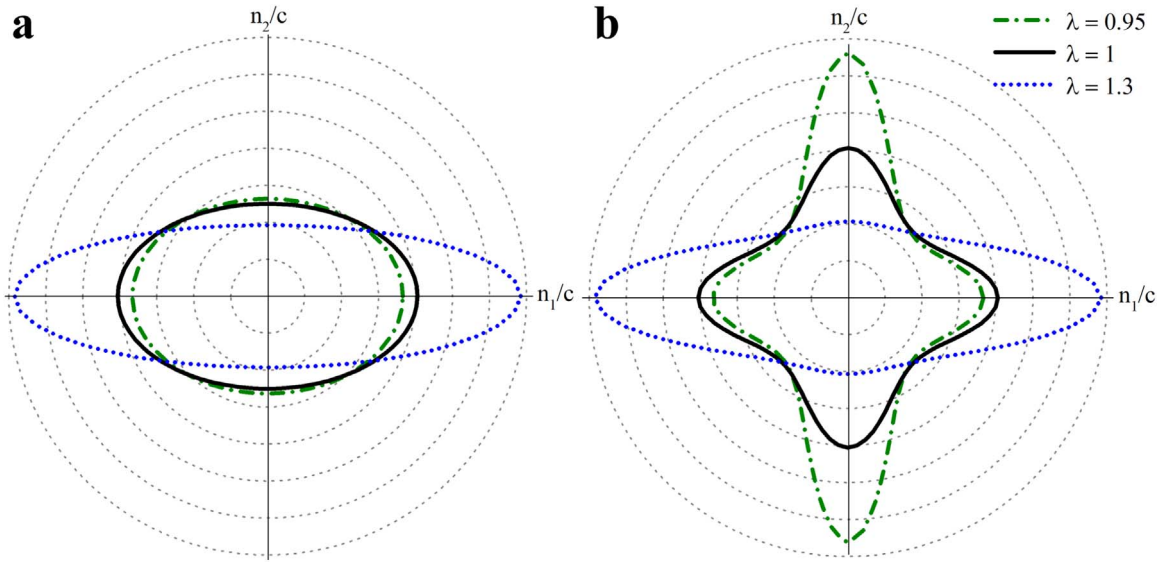

Fig. 2. Slowness curves for (a) out-of-plane and (b) in-plane shear waves propagating in the laminate with $\nu_a = 0.1$, $\mu_a/\mu_b = 20$, and $\rho_{0a}/\rho_{0b} = 1$ under equibiaxial deformation. Scale is 0.4 per division, and the slownesses are normalized by $\sqrt{\overline{\mu}/\overline{\rho}_0}$.

propagation (see Fig. 2(b)). In particular, these directions are expressed as

$$\varphi_0 = \pm\frac{1}{2}\arccos\left(\frac{1-\lambda^6}{4\left(1-\frac{\breve{\mu}}{\overline{\mu}}\right)}\right)+\pi z, \quad z=0,\,1. \tag{50}$$

In the undeformed state, $\varphi_0 = \pm\frac{\pi}{4}, \pm\frac{3\pi}{4}$. Moreover, these directions differ from the principal directions in contrast to the out-of-plane shear wave – the phase velocity of which has maxima in the directions of the principal axes. For example, in the equibiaxially deformed laminate the phase velocity of the out-of-plane shear wave is maximal for the wave propagation along the layers, i.e. for $\mathbf{n} = \pm\mathbf{e}_2$ (see Fig. 2(a)). Note that in the undeformed state the phase velocity of the in-plane shear wave is the same for wave propagation along and perpendicular to the layers, namely Eq. $(41)_2$ yields

$$\overline{c}_{sw}^{(2)} = \sqrt{\breve{\mu}/\overline{\rho}_0}\,. \tag{51}$$

The dispersion relations for long waves in the incompressible laminates are derived from (41)

$$\overline{\omega}_{sw}^{(1)} = \sqrt{b_1/\overline{\rho}_0} \quad \text{and} \quad \overline{\omega}_{sw}^{(2)} = \sqrt{b_2/\overline{\rho}_0} \tag{52}$$

where

$$b_1 = \overline{\mu}\,(\mathbf{k}\cdot\overline{\mathbf{B}}\cdot\mathbf{k}) + (\breve{\mu}-\overline{\mu})(\mathbf{k}\cdot\overline{\mathbf{F}}\cdot\mathbf{m})^2 \quad \text{and} \quad b_2 = b_1 + \frac{\overline{\mu}-\breve{\mu}}{\alpha^2}\left(\frac{4\beta_k^2}{\alpha}-k^2\right)\left(\alpha-\frac{\beta_k^2}{k^2}\right), \tag{53}$$

where $\mathbf{k}$ is the wave vector, $k = |\mathbf{k}|$ is the wave number, and $\beta_k = \mathbf{k}\cdot\overline{\mathbf{F}}^{-T}\cdot\mathbf{m}$.

Now we can find the transmission velocity of a wave packet or the group velocity (Kittel, 2004)

$$\mathbf{v}_g = \nabla_{\mathbf{k}}\,\omega. \tag{54}$$

From (52) and (54), we obtain the explicit formulae for the group velocities in homogenized laminates

$$\mathbf{v}_{sw}^{(1)} = \frac{\overline{\mu}\overline{\mathbf{B}}\cdot\mathbf{n} + (\breve{\mu}-\overline{\mu})(\mathbf{n}\cdot\overline{\mathbf{F}}\cdot\mathbf{m})\overline{\mathbf{F}}\cdot\mathbf{m}}{\sqrt{\overline{\rho}_0 a_1}} \tag{55}$$

and

$$\mathbf{v}_{sw}^{(2)} = \frac{1}{\sqrt{\overline{\rho}_0 a_2}}\left(\overline{\mu}\overline{\mathbf{B}}\cdot\mathbf{n} + (\breve{\mu}-\overline{\mu})(\mathbf{n}\cdot\overline{\mathbf{F}}\cdot\mathbf{m})\overline{\mathbf{F}}\cdot\mathbf{m} + \frac{\overline{\mu}-\breve{\mu}}{\alpha^2}\left(\beta\left(5-\frac{8\beta^2}{\alpha}\right)\overline{\mathbf{F}}^{-T}\cdot\mathbf{m} + \left(\frac{4\beta^4}{\alpha}-\alpha\right)\mathbf{n}\right)\right). \tag{56}$$

To illustrate the derived results (55) and (56), energy curves (Nayfeh, 1995) are plotted in Fig. 3. Fig. 3 shows the energy curves for (a) out-of-plane and (b) in-plane shear waves in the laminate with $\nu_a = 0.1$, $\mu_a/\mu_b = 20$, and $\rho_{0a}/\rho_{0b} = 1$ under equibiaxial deformation. Clearly, the group velocities of the both shear waves strongly depend on the applied deformation and direction of wave

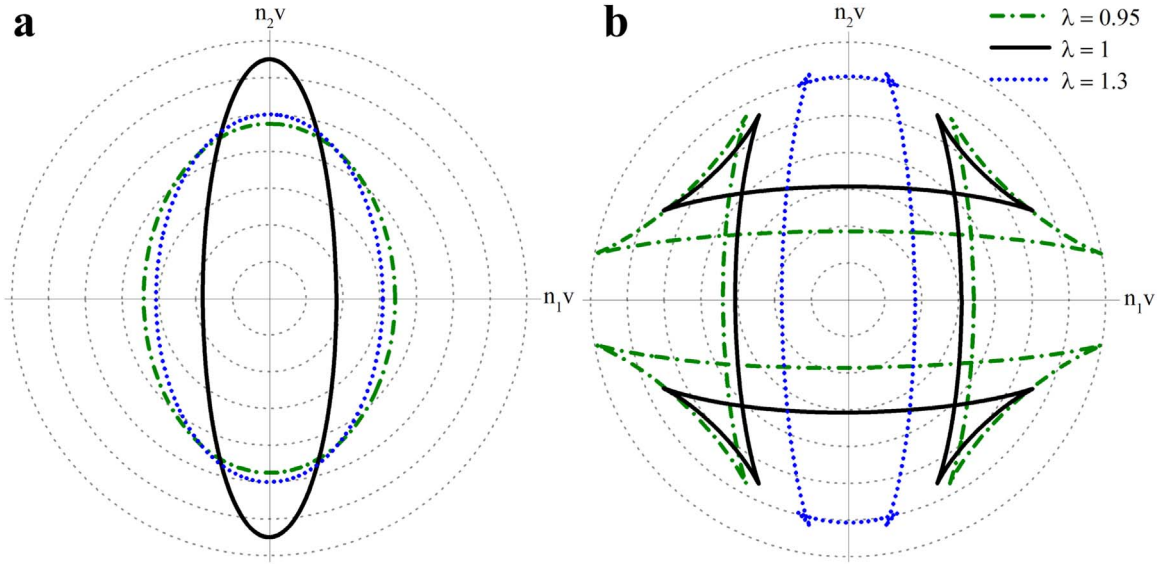

Fig. 3. Energy curves for (a) out-of-plane and (b) in-plane shear waves in the laminate under equibiaxial deformation ($\nu_a = 0.1$, $\mu_a/\mu_b = 20$, and $\rho_{0a}/\rho_{0b} = 1$). Scale is 0.2 per division, where group velocity is normalized by $\sqrt{\overline{\rho}_0/\overline{\mu}}$.

propagation. In particular, an equibiaxial extension increases the group velocity of the out-of-plane shear wave propagating perpendicular to the layers while it decreases the group velocity of the in-plane shear wave propagating in the same direction. An equibiaxial contraction increases group velocities of both the out-of-plane and the in-plane shear waves propagating perpendicular to the layers. Moreover, the energy curves of the in-plane shear waves have the cusps, and position of the cusps is highly tunable by deformation (see Fig. 3(b)). According to Nayfeh (1995) these cusps correspond to regions of null energy. However, for the out-of-plane shear wave the cusps are not observed (see Fig. 3(a)).

3.1.2. Compressible laminates

Next we present long wave estimates for the phase velocities of pressure and shear waves propagating in the direction perpendicular to the layers in the finitely deformed laminate with *compressible* neo-Hookean and Gent phases. Recall (Boulanger et al., 1994) that the phase velocities of shear and pressure waves in the finitely deformed neo-Hookean material for $\mathbf{F}_\xi = \lambda_{1\xi}\mathbf{e}_1 \otimes \mathbf{e}_1 + \lambda_{2\xi}\mathbf{e}_2 \otimes \mathbf{e}_2 + \lambda_{3\xi}\mathbf{e}_3 \otimes \mathbf{e}_3$ and $\mathbf{n} = \mathbf{e}_1$ are the following:

$$c_\xi^s = \lambda_{1\xi}\sqrt{\frac{\mu_\xi}{\rho_{0\xi}}} \quad \text{and} \quad c_\xi^p = \sqrt{\frac{\Lambda_\xi J_\xi^2 + \mu_\xi(1+\lambda_{1\xi}^2)}{\rho_{0\xi}}}. \tag{57}$$

When the wavelength is much larger than the period of the laminate, the sines can be replaced by their arguments and only second order terms are retained from the cosines in Eq. (23), namely

$$\sin\left(\frac{\omega d_\xi}{c_\xi}\right) \simeq \frac{\omega d_\xi}{c_\xi} \quad \text{and} \quad \cos\left(\frac{\omega d_\xi}{c_\xi}\right) \simeq 1 - \frac{\omega^2 d_\xi^2}{2c_\xi^2}. \tag{58}$$

Under this assumption, substitution of (12) and (57) in (23) yields expressions for the phase velocities of shear and pressure waves propagating perpendicular to the layers ($\mathbf{n} = \mathbf{m} = \mathbf{e}_1$) in the finitely deformed layered material with neo-Hookean phases:

$$\overline{c}_{sw} = \overline{\lambda}_1\sqrt{\breve{\mu}/\overline{\rho}_0} \quad \text{and} \quad \overline{c}_{pw} = \overline{\lambda}_1\sqrt{\breve{\Gamma}/\overline{\rho}_0}, \tag{59}$$

where

$$\breve{\Gamma} = (v_a/\Gamma_a + v_b/\Gamma_b)^{-1} \quad \text{and} \quad \Gamma_\xi = \Lambda_\xi(\lambda_{2\xi}\lambda_{3\xi})^2 + \mu_\xi(1+\lambda_{1\xi}^{-2}). \tag{60}$$

For the in-plane tension (27), $\lambda_{2\xi} = \lambda$ and $\lambda_{3\xi} = 1$, while for the equibiaxial deformation (28) $\lambda_{2\xi} = \lambda_{3\xi} = \lambda$.

For the Gent material model, the phase velocities of shear and pressure waves are (Galich and Rudykh, 2015b)

$$c_\xi^s = \lambda_{1\xi}\sqrt{\mu_\xi J_{m\xi}/(\theta_\xi\rho_{0\xi})} \tag{61}$$

and

$$c_\xi^p = \sqrt{\frac{\mu_\xi(1+(\eta_\xi - 2/J_{m\xi})J_\xi^2 + J_{m\xi}\theta_\xi^{-2}(\theta_\xi + 2\lambda_{1\xi}^2)\lambda_{1\xi}^2)}{\rho_{0\xi}}}, \tag{62}$$

where $\theta_\xi = 3 + J_{m_\xi} - \mathbf{F}_\xi\colon\mathbf{F}_\xi$. Hence, substitution of (12), (61) and (62) in (23) together with (58) yields expressions for the phase velocities of shear and pressure waves propagating perpendicular to the layers ($\mathbf{n} = \mathbf{m} = \mathbf{e}_1$) in the finitely deformed layered material with Gent phases, namely

$$\overline{c}_{sw} = \overline{\lambda}_1\sqrt{\breve{\Theta}/\overline{\rho}_0} \quad \text{and} \quad \overline{c}_{pw} = \overline{\lambda}_1\sqrt{\breve{G}/\overline{\rho}_0}, \tag{63}$$

where

$$\breve{\Theta} = \left(\frac{v_a}{\Theta_a} + \frac{v_b}{\Theta_b}\right)^{-1} \quad \text{and} \quad \breve{G} = \left(\frac{v_a}{G_a} + \frac{v_b}{G_b}\right)^{-1}, \tag{64}$$

where $\Theta_\xi = \mu_\xi J_{m\xi}/\theta_\xi$ and

$$G_\xi = \mu_\xi\left(\lambda_{1\xi}^{-2} + \left(\eta_\xi - \frac{2}{J_{m\xi}}\right)(\lambda_{2\xi}\lambda_{3\xi})^2 + J_{m\xi}\theta_\xi^{-2}(\theta_\xi + 2\lambda_{1\xi}^2)\right). \tag{65}$$

Fig. 4 shows a comparison of the long wave estimates (59) and (63) with the exact solution (23) for the waves propagating perpendicular to the layers under equibiaxial deformation. Here and thereafter, we present the normalized frequency $f_n = fd^o\sqrt{\overline{\rho}_0/\breve{\mu}}$, where $f = \omega/(2\pi)$. Remarkably, the long wave estimates (59) and (63) are in excellent agreement with the exact solution (23) for wavelengths exceeding the effective period of the laminate, namely $l \gtrsim \pi d$. For example, for $l = 4d$ the differences in frequencies between the long wave estimates and exact solution are less than 1% for both shear and pressure waves (see Fig. 4).

3.2. Band gap structure

Band gap is a frequency range where waves cannot propagate due to, for example, Bragg scattering (Kushwaha et al., 1993) or/

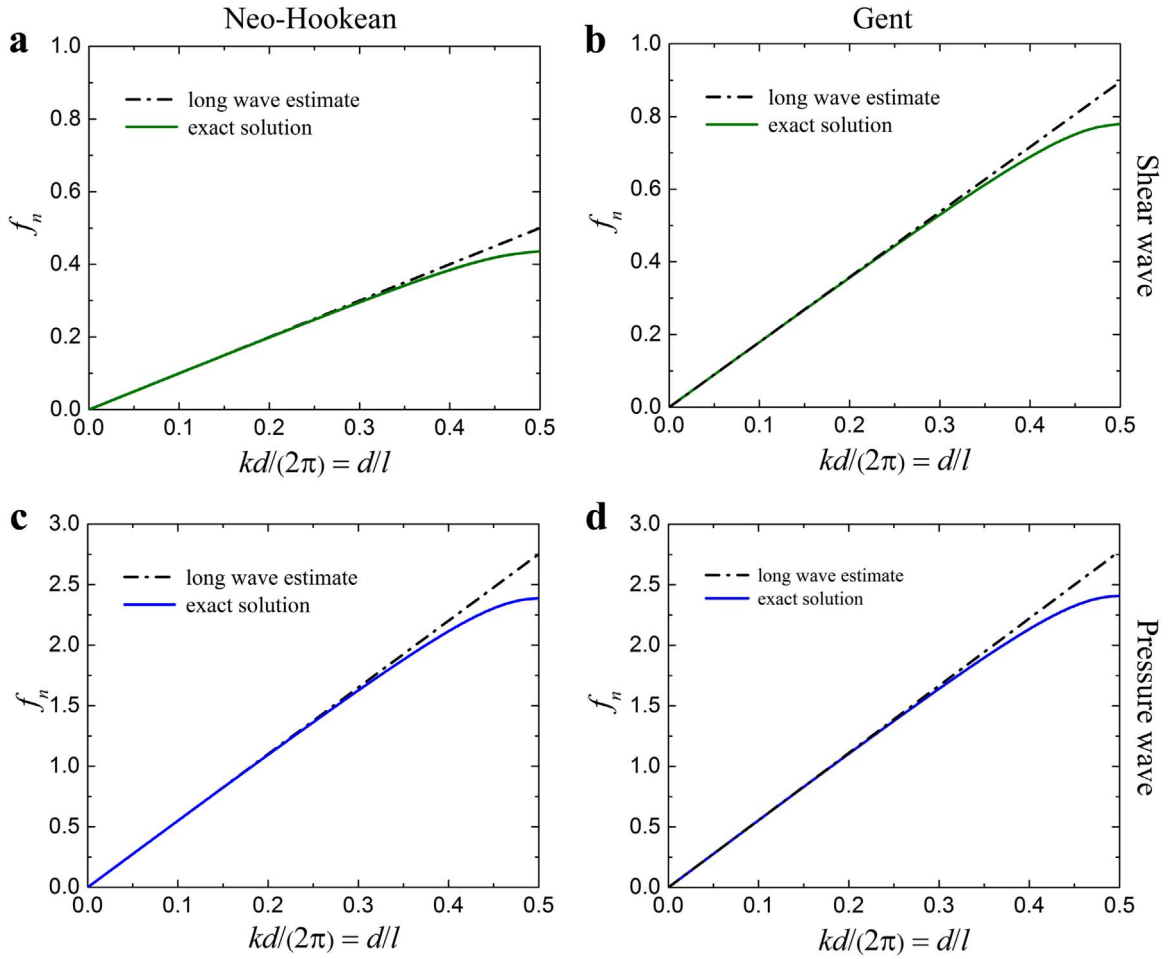

Fig. 4. Comparison of the long wave estimates (59) and (63) with the exact solution (23) for the waves propagating perpendicular to the layers in the laminates with neo-Hookean ((a) and (c)) and Gent ((b) and (d)) phases under equibiaxial deformation ($\lambda = 1.5$). $\nu_a = 0.2$, $\mu_a/\mu_b = 100$, $\rho_{0a}/\rho_{0b} = 1.5$, $\Lambda_a/\mu_a = 10$, $\Lambda_b/\mu_b = 5$, $J_{mb} = 2.5$, and $J_{ma}/J_{mb} = 2$. (a) and (b) correspond to shear waves and (c) and (d) – pressure waves.

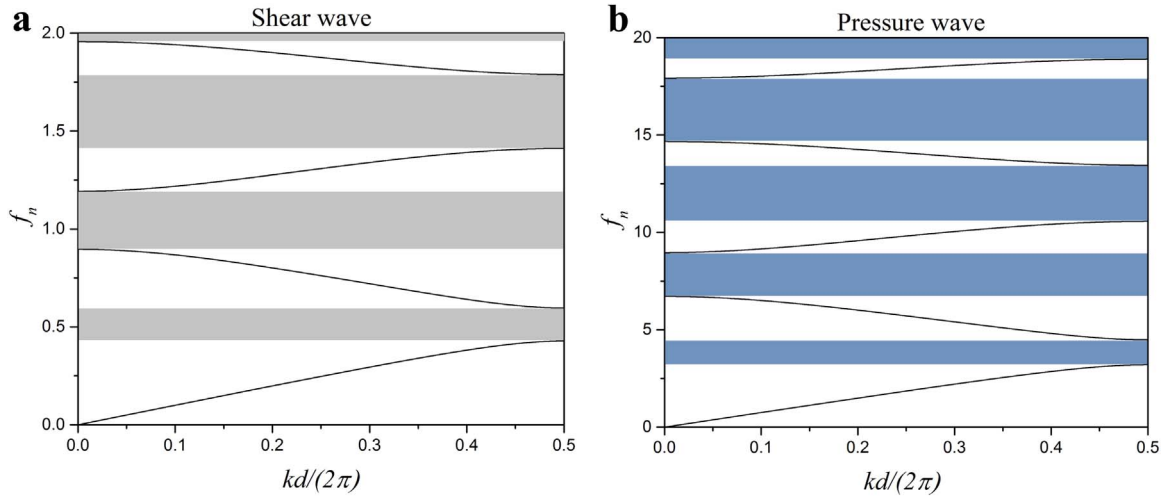

Fig. 5. Dispersion diagrams for shear (a) and pressure (b) waves in the laminate with $\nu_a = 0.3$, $\mu_a/\mu_b = 100$, $\Lambda_a/\mu_a = 100$, $\Lambda_b/\mu_b = 10$, and $\rho_{0a}/\rho_{0b} = 1$ under equibiaxial tension, $\lambda = 1.5$. The shaded areas correspond to the shear (gray) and pressure (blue) wave band gaps. Frequency is normalized as $f_n = \frac{\omega d^0}{2\pi}\sqrt{\bar{\rho}_0/\bar{\mu}}$. (For interpretation of the references to color in this figure caption, the reader is referred to the web version of this paper.)

and local resonance (Auriault and Bonnet, 1985; Auriault, 1994; Liu et al., 2000; Auriault and Boutin, 2012). In case of layered media with high contrast in the mechanical properties between the phases both Bragg scattering and inner resonance of stiffer layer (Auriault and Boutin, 2012) participate in formation of band gaps (Khelif and Adibi, 2016). Mathematically, it corresponds to the situation when wave number k becomes imaginary in the dispersion relation (23), i.e. within a band gap displacement and stress amplitudes exponentially attenuate (see Eqs. (17) and (20)). Fig. 5 illustrates the band gap structures of shear and pressure waves in the finitely deformed laminate with $v_a = 0.3$, $\mu_a/\mu_b = 100$, $\Lambda_a/\mu_a = 100$, $\Lambda_b/\mu_b = 10$, and with identical densities of the phases,[3] i.e. $\rho_{0a}/\rho_{0b} = 1$. The laminate is subjected to equibiaxial tension with the magnitude of the stretch ratio $\lambda = 1.5$. The shaded gray and blue areas correspond to the shear and pressure wave BGs, respectively. Clearly, the shear wave BGs appear earlier (i.e. at lower frequencies) than the pressure wave BGs (compare Fig. 5(a) and (b)); thus, to induce complete BGs at the low-frequency range, one needs to design laminates with pressure wave BGs at the low-frequency range. Next, we identify the key parameters that govern the shear and pressure wave band gaps.

3.2.1. Incompressible laminate

Here we consider the influence of (a) microstructures, (b) deformations, and (c) elastic moduli on the band gap structures in *incompressible* laminates. Recall that incompressible materials support only shear waves; consequently, only shear wave band gaps (SBGs) are considered, while pressure wave BGs (PBG) will be considered in detail in the next section.

(a) *Material geometry*. First, we investigate the influence of the material geometry on SBG structure. Fig. 6(a) presents the width of the first SBG as a function of the volume fraction of phase a. The first SBG has a maximal width for a certain volume fraction v_a; moreover, the maximal width of SBG with corresponding volume fraction of phase a strongly depends on the contrast in shear modulus between the phases (compare Fig. 6(a) and (b)). Thus, for the contrast in shear modulus of $\mu_a/\mu_b = 10$, the maximal width of the first SBG is $\Delta f_n = 0.41$ with $v_a = 0.76$; while for the contrast in shear modulus of $\mu_a/\mu_b = 1000$, the SBG width significantly increases up to $\Delta f_n = 2.25$, and the corresponding volume fraction shifts to $v_a = 0.97$. It is clear that an increase in the shear modulus contrast widens the maximal SBG width. Thus, wide SBGs can be achieved by composing laminates with thin soft layers embedded in the stiff phase ($v_b = 0.03$ in Fig. 6(b)). As expected SBGs disappear when $v_a = 0$ or 1.

(b) *Deformation*. Next, we analyze the influence of deformation on SBGs. We start from the consideration of laminates with phases characterized by weak stiffening, which can be described by neo-Hookean model (29). Substitution of the corresponding phase velocities $(57)_1$ into the dispersion relation (23), together with the deformation induced change in geometry (12), yields

$$\cos k\bar{\lambda}_1 d^o = \cos\left(\omega d_a^o \sqrt{\frac{\rho_{0a}}{\mu_a}}\right)\cos\left(\omega d_b^o \sqrt{\frac{\rho_{0b}}{\mu_b}}\right) - \frac{1}{2}\left(\sqrt{\frac{\rho_{0a}\mu_a}{\rho_{0b}\mu_b}} + \sqrt{\frac{\rho_{0b}\mu_b}{\rho_{0a}\mu_a}}\right)\sin\left(\omega d_a^o \sqrt{\frac{\rho_{0a}}{\mu_a}}\right)\sin\left(\omega d_b^o \sqrt{\frac{\rho_{0b}}{\mu_b}}\right). \tag{66}$$

This result clearly shows that SBGs in layered materials with neo-Hookean phases do not depend on deformation. This is due to the equal contribution of two competing effects induced by deformation: (i) the change in the phase properties (i.e. $c_\xi^{nH}/c_\xi^o = \lambda_{1\xi}$, where c_ξ^{nH} and c_ξ^o are the phase velocities in the deformed and undeformed material) and (ii) change in the layer thicknesses (i.e. $d_\xi/d_\xi^o = \lambda_{1\xi}$). Clearly, any deformation induced change in the geometry is fully compensated by the change in the phase velocity.

However, for laminates with phases exhibiting stronger stiffening (such as Gent phases), the deformation induced change in the effective properties prevails over the geometry changes. The phase velocities of the shear waves in a deformed Gent material are larger than in the identically deformed neo-Hookean material (i.e. $c_\xi^G/c_\xi^{nH} = \sqrt{J_{m\xi}/\theta_\xi} > 1$) while the changes in the geometry are the same. Fig. 7 presents the relative changes in the phase velocities of the shear waves as functions of the stretch for the neo-Hookean and Gent phases under in-plane tension. Clearly, for the contraction ($\lambda < 1$), the phase velocities of the shear waves in the Gent phase increase more significantly than in the neo-Hookean phase. For the extension ($\lambda > 1$), the phase velocities of the shear waves in the Gent phase decrease in the beginning; however, the phase velocity starts to grow as the stiffening effect becomes more pronounced with an increase in deformation. Eventually, the phase velocity becomes larger than the one in the undeformed material. This corresponds to a certain stretch ratio $\lambda^* < \lambda^{lock}$ (see Fig. 7); the expressions for this stretch ratio are

$$\lambda_{pt}^* = \sqrt{1 + J_m} \tag{67}$$

for the in-plane tension and

$$\lambda_{bt}^* = \frac{1}{2}\sqrt{1 + J_m + \sqrt{9 + (10 + J_m)J_m}} \tag{68}$$

for the equibiaxial extension. Since in laminates with Gent phases the deformation induced change in material properties (i.e. $c_\xi^G/c_\xi^o = \lambda_{1\xi}\sqrt{J_{m\xi}/\theta_\xi}$) is not fully compensated by the change in the geometry (i.e. $d_\xi/d_\xi^o = \lambda_{1\xi}$), the tunability of SBGs by deformation is observed.

Fig. 8 illustrates the dependence of SBGs on in-plane ((a) and (c)) and equibiaxial ((b) and (d)) deformations for the layered materials with Gent phases. The lock-up stretches for $J_m = 2.5$ are $\lambda_-^{lock} = 0.48$ and $\lambda_+^{lock} = 2.07$ for the in-plane deformation; and $\lambda_-^{lock} = 0.68$ and $\lambda_+^{lock} = 1.64$ for the equibiaxial deformation. We observe that SBGs shift towards higher frequencies and widen as the lock-up stretch ratio is approached. In particular, for the laminate with $v_a = 0.3$, $\mu_a/\mu_b = 100$, $J_{ma} = 5$, and $J_{mb} = 2.5$ the first SBG widens from $\Delta f_n = 0.16$ up to $\Delta f_n = 0.49$ and its lower boundary shifts from $f_n = 0.43$ up to $f_n = 1.35$ by application of the in-plane

[3] Typical deformable polymers are characterized by low densities that change only slightly from polymer to polymer. Therefore, we present the results for laminates with similar or identical phase densities; the values of the density contrast ratio are specified in each example.

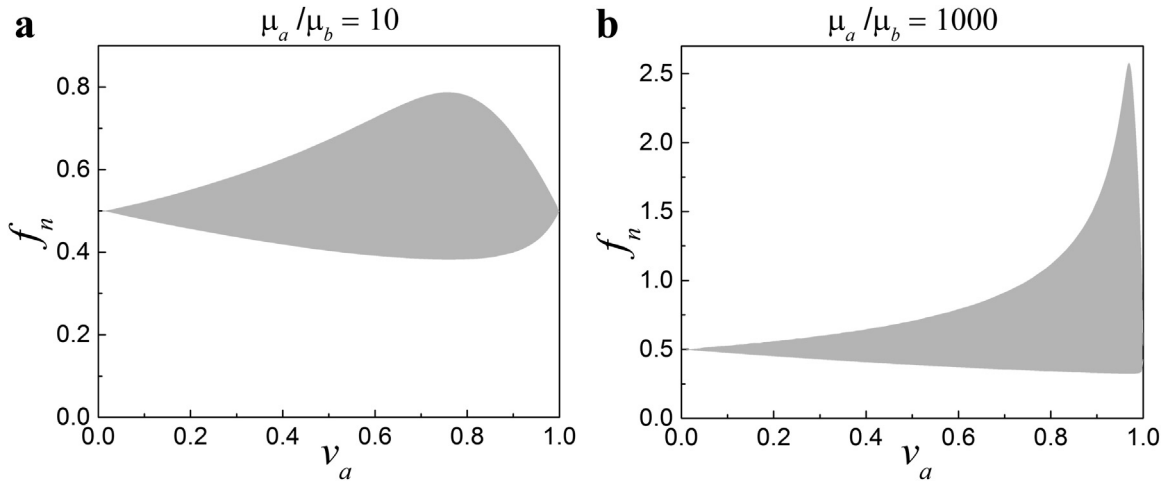

Fig. 6. First shear wave band gap vs. volume fraction of phase a for layered materials in undeformed state with (a) $\mu_a/\mu_b = 10$ and (b) $\mu_a/\mu_b = 1000$; $\rho_{0a}/\rho_{0b} = 1$.

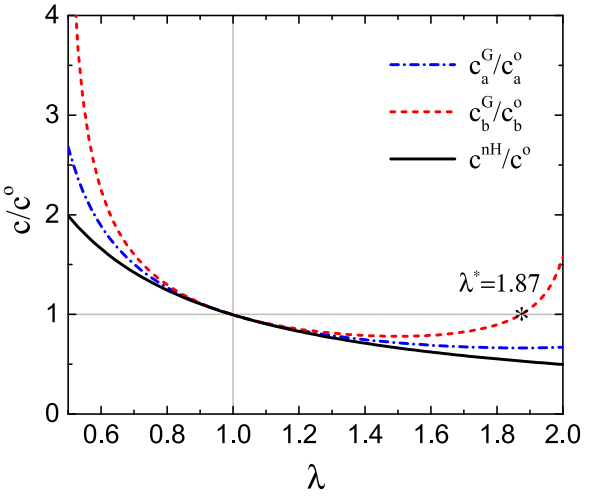

Fig. 7. Relative change in the phase velocities of shear waves as functions of in-plane tension for laminates with $\nu_a = 0.97$, $\mu_a/\mu_b = 1000$, $J_{ma} = 5$, $J_{mb} = 2.5$, and $\rho_{0a}/\rho_{0b} = 1$.

deformation of the magnitude $\lambda = 0.5$ or $\lambda = 2$ (see Fig. 8(a)). The equibiaxial deformation of magnitude $\lambda = 0.70$ or $\lambda = 1.58$ widens the first SBG from $\Delta f_n = 0.16$ up to $\Delta f_n = 0.42$ and shifts its lower boundary from $f_n = 0.43$ up to $f_n = 1.14$ (see Fig. 8(b)). Fig. 8(c) and (d) show the first SBG as a function of the stretch ratio for the in-plane (c) and equibiaxial (d) deformations for the laminate with the volume fraction producing a maximal width of the first SBG in the undeformed laminate, namely $\nu_a = 0.97$ and $\mu_a/\mu_b = 1000$. Consistent with the previous observations the first SBG widens and shifts towards higher frequencies once the lock-up stretches are attained. In particular, lower boundary of the first SBG shifts from $f_n = 0.33$ up to $f_n = 1.00$ and its width increases from $\Delta f_n = 2.25$ up to $\Delta f_n = 2.73$ in the laminate undergoing the in-plane contraction with $\lambda = 0.5$ or extension with $\lambda = 2$ (Fig. 8(c)). Clearly, equibiaxial deformation has a more pronounced effect on SBGs as compared to the in-plane deformation (compare Fig. 8(a) vs. (b) and (c) vs. (d)). Remarkably, contraction ($\lambda < 1$) and extension ($\lambda > 1$) of the laminate with Gent phases influence SBGs in similar ways, namely any homogeneous deformations considered here widen and shift up SBGs towards higher frequencies (see Fig. 8). This happens because for both contraction ($\lambda < 1$) and extension ($\lambda > 1$), the stiffening leads to an increase in the phase velocities of the Gent phases compared to the phase velocities of the neo-Hookean constituents, i.e. $c_\xi^G/c_\xi^{nH} = \sqrt{J_{m\xi}/\theta_\xi} > 1$ (see Fig. 7), whereas the deformation induced geometry changes are identical for laminates with weak and strong stiffening effects, i.e. $d_\xi/d_\xi^o = \lambda_{1\xi}$. For example, the in-plane contraction of the magnitude $\lambda = 0.5$ increases the phase velocities in the layers a and b up to $c_a^G/c_a^o = 2.7$ and $c_b^G/c_b^o = 6.3$, respectively, whereas the layer thicknesses increase up to $d/d^o = 2$ only (see Fig. 7). Again, the in-plane extension of the magnitude $\lambda = 2$ decreases the phase velocity in the layer a down to $c_a^G/c_a^o = 0.7$ and increases it up to $c_b^G/c_b^o = 1.6$ in the layer b, whereas the layer thicknesses decrease down to $d/d^o = 0.5$ (see Fig. 7). Note that for the in-plane tension of magnitude $\lambda = 0.5$ or $\lambda = 2$, the phase velocities in Gent phases increase by the same value compared to the phase velocities of the neo-Hookean phases, namely $c_a^G/c_a^{nH}|_{\lambda=0.5} = c_a^G/c_a^{nH}|_{\lambda=2} = 1.35$ and $c_b^G/c_b^{nH}|_{\lambda=0.5} = c_b^G/c_b^{nH}|_{\lambda=2} = 3.16$. This together with the identical deformation induced change in the geometry leads to the identical width and position of the SBGs for these values of the stretch ratio.

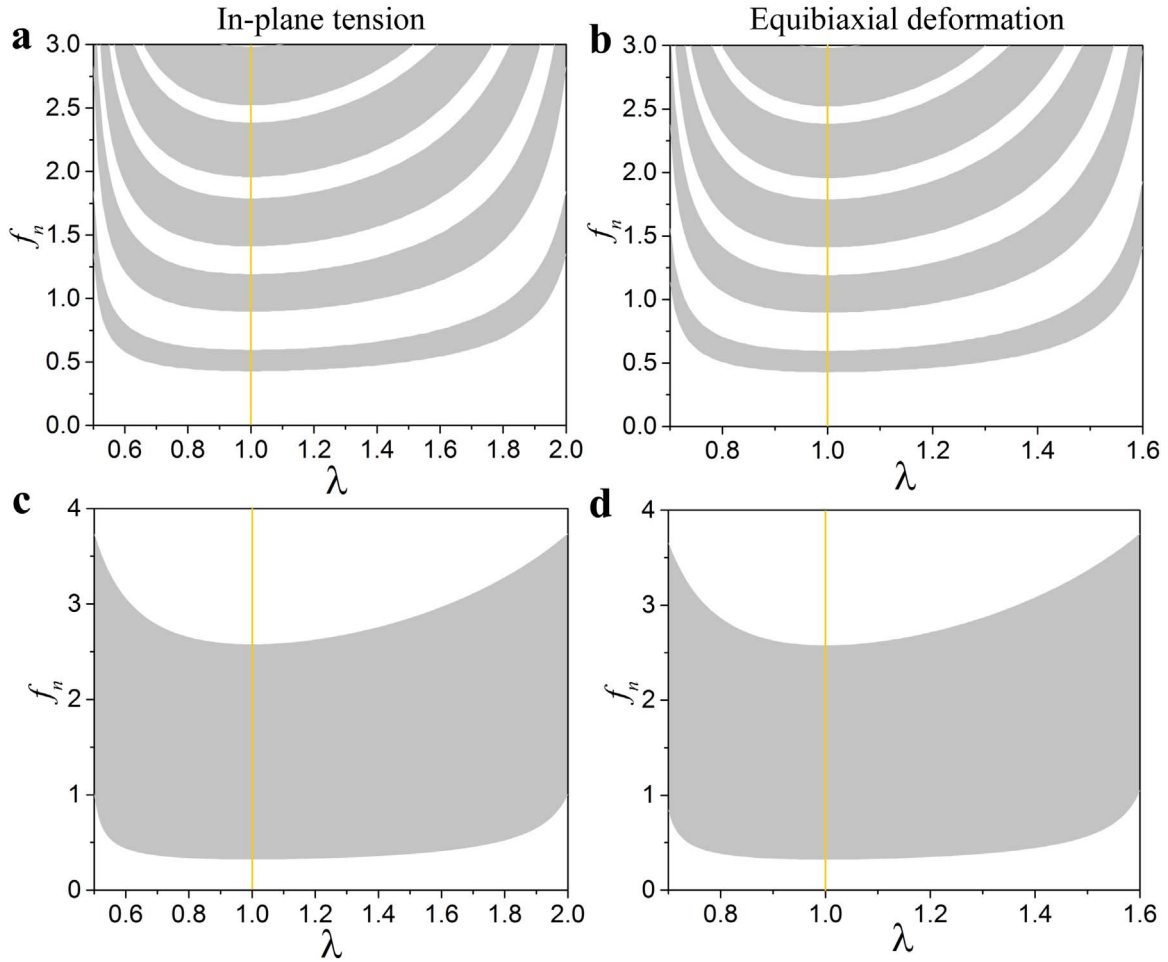

Fig. 8. Shear wave band gaps vs. in-plane ((a) and (c)) and equibiaxial ((b) and (d)) deformations for the layered materials with Gent phases, namely $\rho_{0a}/\rho_{0b} = 1$, $J_{ma} = 5$, $J_{mb} = 2.5$, $\nu_a = 0.3$, $\mu_a/\mu_b = 100$ ((a) and (b)) and $\nu_a = 0.97$, $\mu_a/\mu_b = 1000$ ((c) and (d)).

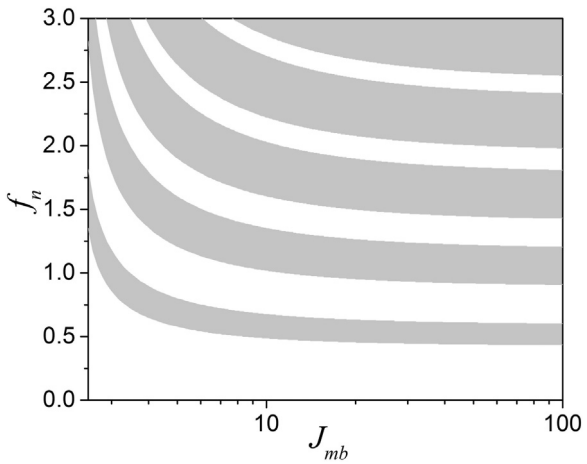

Fig. 9. Shear wave band gaps as a function of locking parameter J_{mb} for the layered material with $\nu_a = 0.3$, $J_{ma} = 100$, $\rho_{0a}/\rho_{0b} = 1$, and $\mu_a/\mu_b = 100$ subjected to the in-plane tension of the magnitude $\lambda = 2$.

To illustrate the influence of the stiffening of the laminate constituents on the SBGs, we present SBGs as functions of locking parameter J_{mb} for the layered material with $\nu_a = 0.3$, $J_{ma} = 100$, and $\mu_a/\mu_b = 100$ subjected to the in-plane tension of the magnitude $\lambda = 2$ in Fig. 9. We observe that SBGs widen and shift towards higher frequencies with a decrease in the locking parameter J_{mb}. In

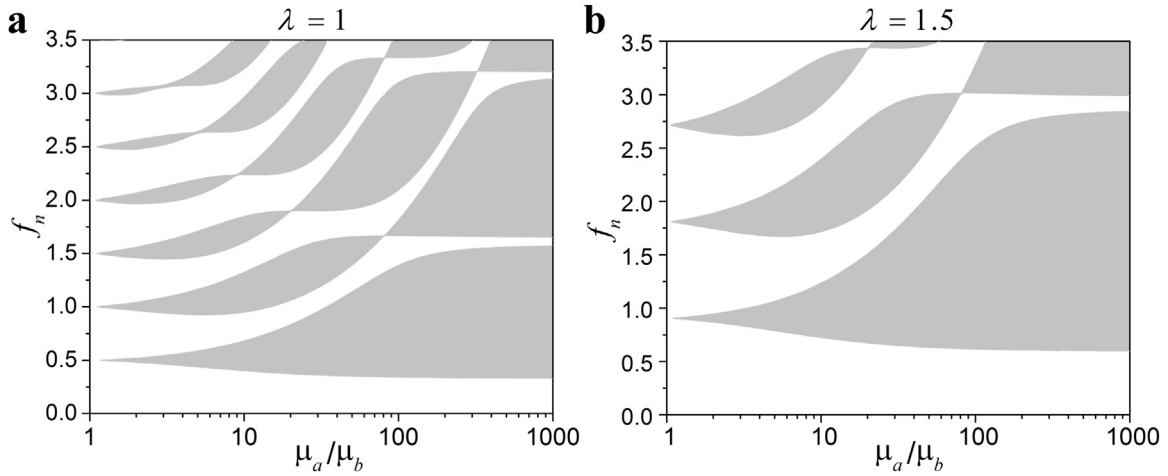

Fig. 10. Shear band gaps vs. shear modulus contrast for the layered material with $\nu_a = 0.9$, $\rho_{0a}/\rho_{0b} = 1$, and $J_{ma} = J_{mb} = 1$ in the undeformed state (a) and the one subjected to the in-plane tension with $\lambda = 1.5$ (b).

particular, the lower boundary of the first SBG shifts from $f_n = 0.44$ up to $f_n = 1.35$ and its width increases from $\Delta f_n = 0.16$ up to $\Delta f_n = 0.46$ when locking parameter of phase b decreases from $J_{mb} = 100$ down to $J_{mb} = 2.5$. This happens because the lock-up stretch ratio (34) decreases together with J_{mb}, leading to the significant increase in the phase velocity of shear wave in the phase b (see Eq. (61)).

(c) *Shear modulus contrast*. To illustrate the influence of the shear modulus contrast of the phases on SBGs, we present SBGs as functions of the shear modulus contrast for the laminates with $\nu_a = 0.9$ and $J_{m\xi} = 1$ in Fig. 10. The corresponding lock-up stretch ratio is $\lambda = 1.62$. The SBGs of the undeformed ($\lambda = 1$) laminate and the one subjected to the in-plane tension with $\lambda = 1.5$ are presented in Fig. 10(a) and (b), respectively. Fig. 10(a) shows that the first SBG rapidly widens with an increase in the contrast from 1 to ~100, after that the upper boundary flattens, and the SBG width changes slowly with further increase in the shear modulus contrast. The second and the following SBGs close at certain values of the shear modulus contrast. For example, the third SBG closes when $\mu_a/\mu_b = 20$ and $\mu_a/\mu_b = 322$; however, the SBG reopens again if the shear modulus contrast increases. For laminates with phases exhibiting strong stiffening (such as Gent phases), these BGs shift towards higher frequencies for any shear modulus contrast with application of deformation. In particular, the first SBG widens from $\Delta f_n = 0.79$ up to $\Delta f_n = 1.44$ and its lower boundary shifts from $f_n = 0.35$ up to $f_n = 0.63$ in the laminate with $\mu_a/\mu_b = 50$ subjected to the in-plane extension of the magnitude $\lambda = 1.5$ (Fig. 10(b)).

3.2.2. Compressible laminates

To analyze the pressure wave BGs (PBGs), we consider periodic layered materials with *compressible* phases to ensure the existence of pressure waves. Fig. 11 shows pressure and shear wave BGs as functions of the volume fraction of phase a in the undeformed and deformed laminates. Here and thereafter, gray, blue, and black colors correspond to the shear wave, pressure wave,

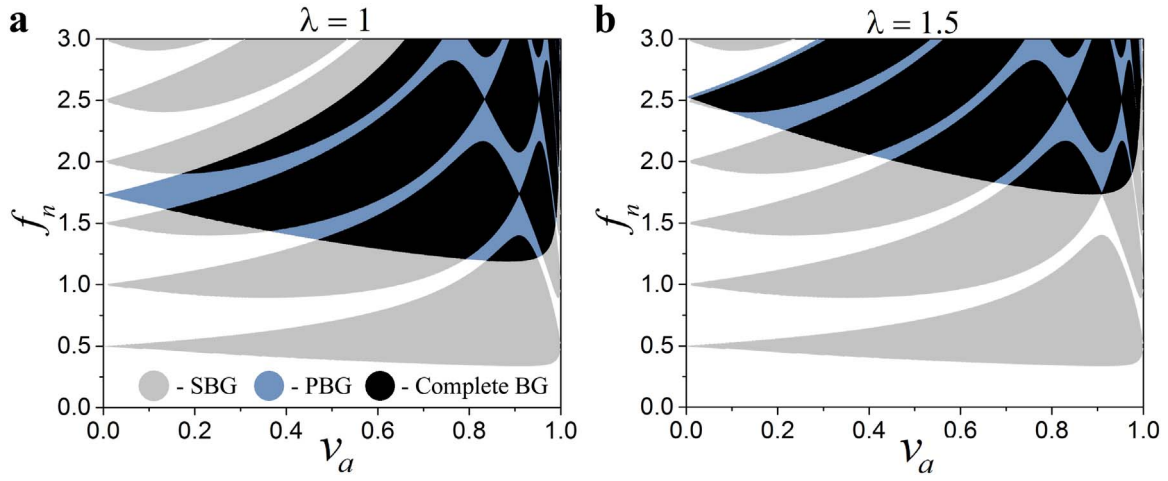

Fig. 11. Band gaps vs. volume fraction of the phase a in the undeformed laminate (a) and the one subjected to the in-plane tension of the magnitude $\lambda = 1.5$ (b) with $\mu_a/\mu_b = 100$, $\Lambda_a/\mu_a = 1000$, $\Lambda_b/\mu_b = 10$, and $\rho_{0a}/\rho_{0b} = 1$. The gray, blue, and black colors correspond to the shear wave, pressure wave, and complete BGs, respectively. (For interpretation of the references to color in this figure caption, the reader is referred to the web version of this paper.)

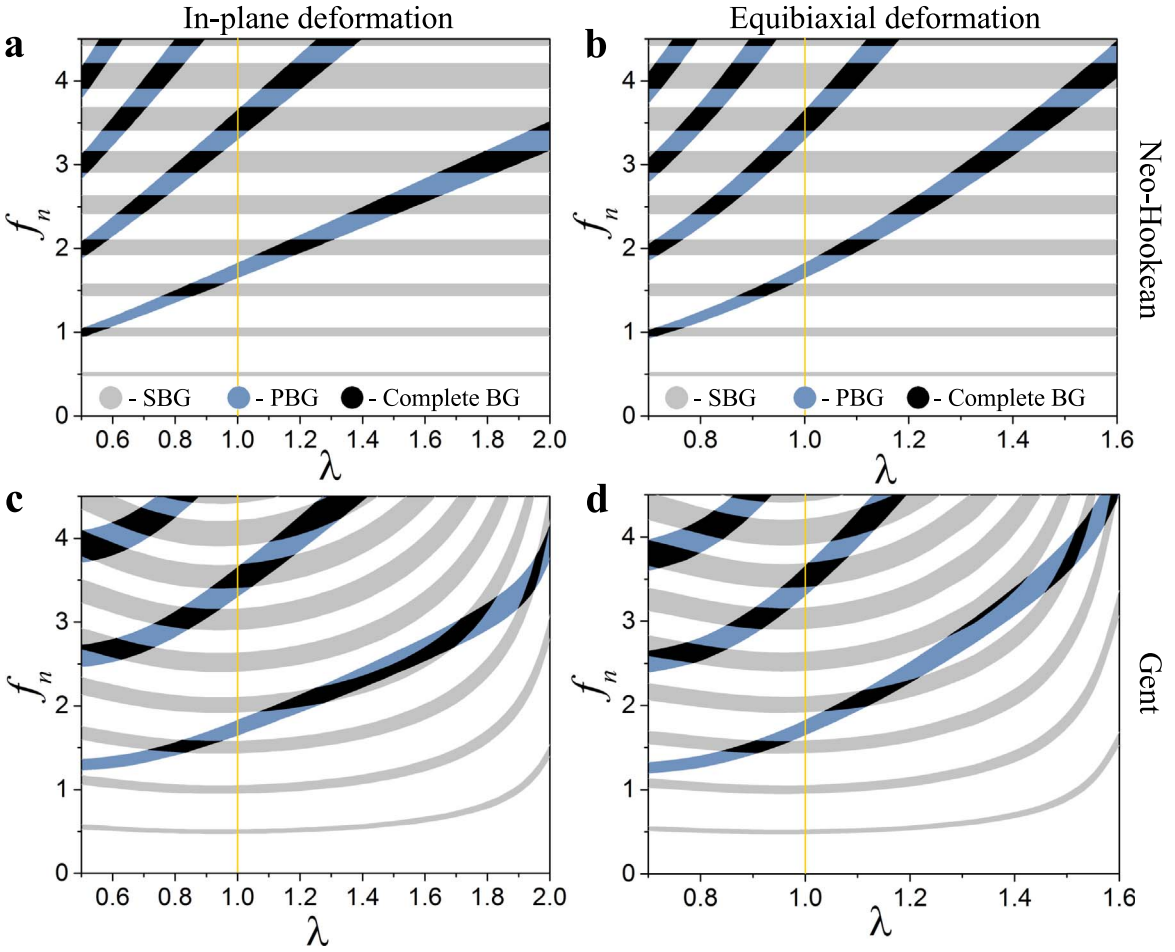

Fig. 12. Band gaps vs. in-plane ((a) and (c)) and equibiaxial ((b) and (d)) deformation for laminates with $v_a = 0.1$, $\mu_a/\mu_b = 100$, $\Lambda_a/\mu_a = 1000$, $\Lambda_b/\mu_b = 10$, and $\rho_{0a}/\rho_{0b} = 1$. (a) and (b) refer to the laminate with neo-Hookean phases and (c) and (d) refer to the laminate with Gent phases having $J_{ma} = 5$ and $J_{mb} = 2.5$.

and *complete* BGs, respectively. We refer to *complete* BGs when both pressure and shear waves cannot propagate. We find that the first PBG has a maximal width for a certain volume fraction v_a depending on the contrast in shear moduli and compressibility of each phase. Thus, different complete BGs can be tailored by varying the initial material properties and geometry.

In the case of shear waves, the ratio of acoustic impedances z_a/z_b is independent of deformation, although the acoustic impedances $z_\xi = \rho_\xi c_\xi$ for both phases are functions of the principal stretches. Substitution of the corresponding phase velocities $(57)_1$, geometry changes (12), and densities $\rho_\xi = J_\xi^{-1}\rho_{0\xi}$ into (23) together with the boundary conditions (25), producing relations $\lambda_{2a} = \lambda_{2b}$ and $\lambda_{3a} = \lambda_{3b}$, yields the dispersion relation (66). Consequently, the SBGs are not influenced by deformation in the laminates with compressible neo-Hookean phases. Similarly to the laminates with incompressible neo-Hookean phases, the deformation induced changes in the material properties are fully compensated by the changes in the geometry.

In the case of pressure waves, the dominant factor influencing PBGs is the deformation induced change in the geometry. This is due to the fact that the phase velocities of pressure waves in neo-Hookean materials change very slowly with the deformation; moreover, the change is negligible in the case of nearly incompressible materials (see Eq. $(57)_2$). A comparison of the BGs in the undeformed laminates (Fig. 11(a)) and the BGs in the laminates subjected to the in-plane tension, $\lambda = 1.5$ (Fig. 11(b)), shows that the applied deformation does not change the SBGs while it significantly influences the PBGs.

To clarify how the pressure wave and complete BGs depend on deformation in the laminates with compressible phases exhibiting weak and strong stiffening, we present these BGs as functions of the applied stretch ratio in Fig. 12. Fig. 12(a) and (b) illustrate how the in-plane (27) and equibiaxial deformations (28) of the layered material with neo-Hookean phases influence the BG structure. We observe that PBGs narrow and shift towards lower frequencies in the laminate undergoing contraction while extension of the laminate widens and shifts PBGs towards higher frequencies. In particular, the lower boundary of the first PBG shifts from $f_n = 1.65$ up to $f_n = 3.17$ and its width increases from $\Delta f_n = 0.18$ up to $\Delta f_n = 0.34$ in the laminate subjected to the in-plane extension of the magnitude $\lambda = 2$ (see Fig. 12(a)). The equibiaxial deformation has a more pronounced effect on the PBGs, in particular, the equibiaxial extension of the magnitude $\lambda = 1.6$ shifts the lower boundary of the first PBG from $f_n = 1.65$ up to $f_n = 4.04$ and widens it from $\Delta f_n = 0.18$ up to $\Delta f_n = 0.44$ (see Fig. 12(b)). Remarkably, complete BGs can be induced in a required frequency range by

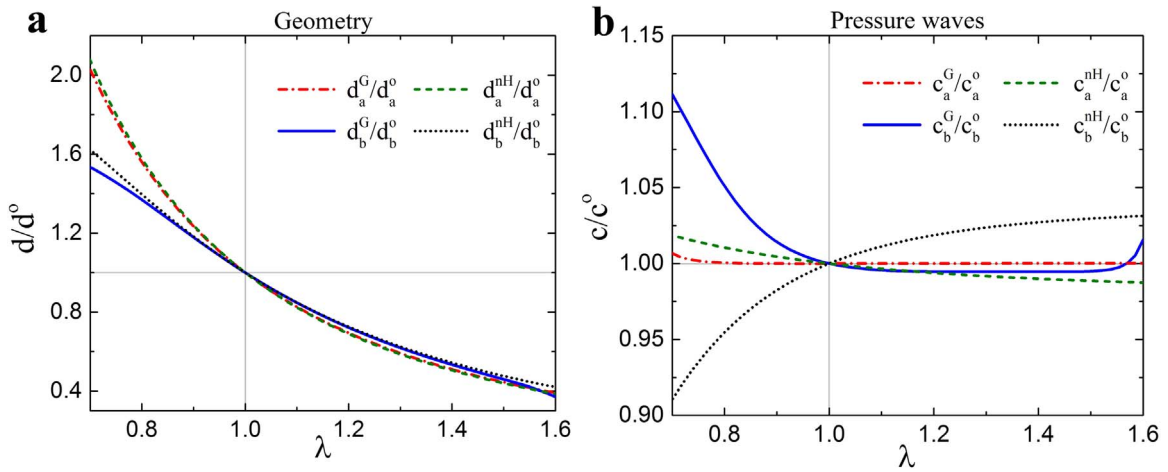

Fig. 13. Relative change in thicknesses of the layers (a) and phase velocities of pressure (b) waves as functions of equibiaxial deformation for the laminates with $\nu_a = 0.1$, $\mu_a/\mu_b = 100$, $\Lambda_a/\mu_a = 1000$, $\Lambda_b/\mu_b = 10$, $J_{ma} = 5$, $J_{mb} = 2.5$, and $\rho_{0a}/\rho_{0b} = 1$. (For interpretation of the references to color in this figure caption, the reader is referred to the web version of this paper.)

deformation while the undeformed laminates do not produce complete BGs in that range. For example, the laminate with $\nu_a = 0.1$, $\mu_a/\mu_b = 100$, $\Lambda_a/\mu_a = 1000$ and $\Lambda_b/\mu_b = 10$ has no complete BGs (in the considered frequency range) in the undeformed state while it has the complete BG of width $\Delta f_n = 0.15$ when subjected to the in-plane contraction of the stretch ratio magnitude $\lambda = 0.85$ (see Fig. 12(a)). In contrast to the in-plane tension, for the equibiaxial deformation we have more "islands" of the complete BGs in the same range of deformation, however, these "islands" are smaller (compare Fig. 12(a) and (b)).

Fig. 12(c) and (d) illustrate how the in-plane (27) and equibiaxial deformations (28) of the layered material with compressible Gent phases influence the BG structure. We observe that in the laminate undergoing in-plane contraction PBGs shift towards lower frequencies less than in laminates with neo-Hookean phases (compare Fig. 12(a) and (c)). In particular, the lower boundary of the first PBG shifts from $f_n = 0.94$ up to $f_n = 1.23$ due to the stiffening of the laminate induced by the in-plane contraction of the magnitude $\lambda = 0.5$. Analogously, the equibiaxial contraction of the laminate with Gent phases shifts PBGs towards lower frequencies less than in the laminate with neo-Hookean phases (compare Fig. 12(b) and (d)). Specifically, the lower boundary of the second PBG shifts from $f_n = 1.86$ up to $f_n = 2.39$ because the laminate under the equibiaxial contraction of the magnitude $\lambda = 0.7$ significantly stiffens. Similar to the effect of contraction in the laminate with Gent phases, the extension induced stiffening shifts PBGs towards higher frequencies compared to the laminates with neo-Hookean phases. In particular, the lower boundary of the first PBG shifts from $f_n = 3.17$ up to $f_n = 3.68$ in the laminate with Gent phases undergoing the in-plane extension of the magnitude $\lambda = 2$ (compare Fig. 12(a) and (c)).

Next, let us consider the mechanisms governing the PBGs in the finitely deformed compressible laminates exhibiting weak and strong stiffening. Fig. 13 presents the relative changes in the thicknesses of the layers (a), and the relative changes in the phase velocities of pressure waves (b) in each layer as functions of the stretch ratio. The example is given for the laminates with neo-Hookean and Gent phases subjected to equibiaxial deformation. The laminate parameters are $\nu_a = 0.1$, $\mu_a/\mu_b = 100$, $\Lambda_a/\mu_a = 1000$, $\Lambda_b/\mu_b = 10$, $J_{ma} = 5$, and $J_{mb} = 2.5$. The corresponding dependence of the BGs on deformation is presented in Fig. 12(b) and (d). A comparison of Fig. 12(b) and (d) together with Fig. 13 shows a correlation between the position of PBGs and changes in the geometry and phase velocities of the layers. In particular, we observe that in the laminate with Gent phases undergoing equibiaxial contraction, the phase velocity of the pressure wave in the highly compressible Gent phase increases while it decreases for the highly compressible neo-Hookean phase (compare continuous blue and dotted black curves in Fig. 13(b)). For example, for the equibiaxial contraction of the magnitude $\lambda = 0.7$ the changes in the pressure wave velocities are $c_b^G/c_b^o = 1.11$ and $c_b^{nH}/c_b^o = 0.91$ for the highly compressible Gent and neo-Hookean phases, respectively. On the other hand, the layer thickness of the highly compressible Gent phase increases less than for the neo-Hookean phase, namely $d_b^G/d_b^o = 1.53$ and $d_b^{nH}/d_b^o = 1.62$ for the laminate subjected to the equibiaxial contraction of $\lambda = 0.7$ (compare continuous blue and dotted black curves in Fig. 13(a)). As a result, the PBGs in the laminates with Gent phases shift towards lower frequencies less than in the laminate with neo-Hookean phases. For the equibiaxial extension of the magnitude $\lambda = 1.6$, the changes in the pressure wave velocities are $c_b^G/c_b^o = 1.02$ and $c_b^{nH}/c_b^o = 1.03$ for the highly compressible Gent and neo-Hookean phases, respectively (Fig. 13(b)); whereas the changes in the layer thicknesses are $d_b^G/d_b^o = 0.37$ and $d_b^{nH}/d_b^o = 0.42$ (Fig. 13(a)). Although the difference in the phase velocities and layer thicknesses between the Gent and neo-Hookean phases is relatively small, the lower boundary of the first PBG shifts from $f_n = 4.04$ in the laminate with neo-Hookean phases up to $f_n = 4.50$ in the laminate with Gent phases undergoing the equibiaxial extension of the magnitude $\lambda = 1.6$ (see Fig. 12(b) and (d)). This happens because of the nonlinear dependence of PBGs on the changes in the material properties and geometry induced by deformation, especially in the case of the extreme deformations approaching the lock-up state ($\lambda^{lock} = 1.64$).

Finally, we consider the influence of compressibility of the laminate constituents on the BGs. Fig. 14 shows BGs as a function of compressibility of the thin softer layers embedded in the nearly incompressible stiffer phase. The results for the undeformed laminate are presented in Fig. 14(a) while the response of the laminate subjected to the equibiaxial compression ($\lambda = 0.5$) is shown in

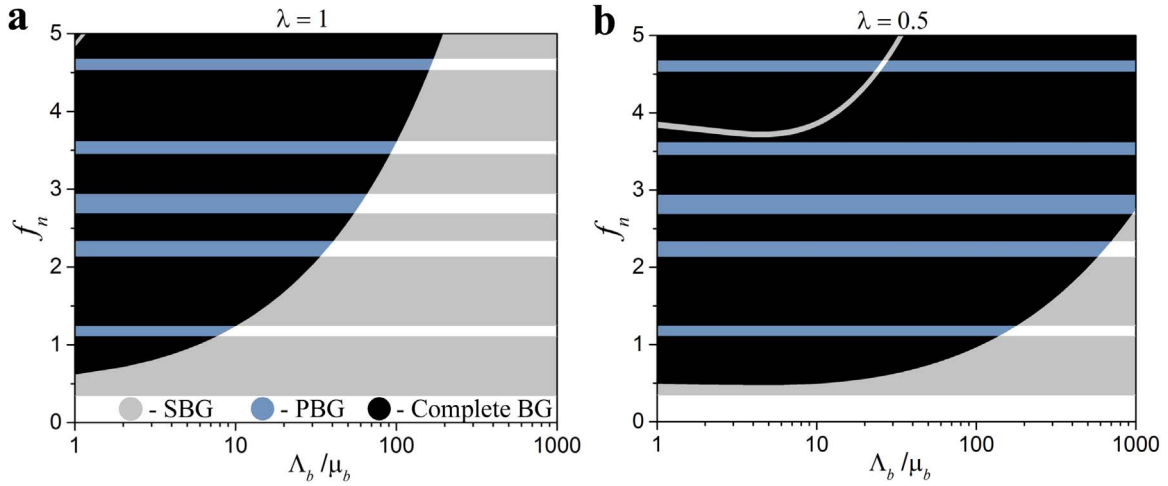

Fig. 14. Band gaps vs. compressibility of the phase b for the laminate with $v_a = 0.96$, $\mu_a/\mu_b = 100$, $\Lambda_a/\mu_a = 1000$, and $\rho_{0a}/\rho_{0b} = 1$ in the undeformed state (a) and the one subjected to the equibiaxial compression, $\lambda = 0.5$ (b).

Fig. 14(b). We observe complete BGs in low-frequency range when compressibility of softer phase increases (i.e. Λ_b/μ_b decreases). For example, for the undeformed laminate with $\Lambda_b/\mu_b = 10$ we observe the first complete BG of width $\Delta f_n = 0.89$ with the lower boundary at $f_n = 1.25$, while for $\Lambda_b/\mu_b > 35$ there are no complete BGs in the considered frequency range (see Fig. 14(a)). Furthermore, the maximal width and position of the lowest complete BG vary depending on the applied deformation; thus, for the laminate with $\Lambda_b/\mu_b = 10$ undergoing equibiaxial contraction ($\lambda = 0.5$), the lowest complete BG has width $\Delta f_n = 0.61$ with the lower boundary at $f_n = 0.50$ (see Fig. 14(b)). Note that an increase in compressibility of the thin layers results in a shift of PBGs towards lower frequencies, producing complete BGs at the low-frequency range. Thus, the wide complete BGs can be realized by composing laminates of a nearly incompressible matrix and highly compressible thin layers.

Fig. 15 shows BGs as functions of deformations for the laminates with both highly compressible phases exhibiting weak ((a) and (c)) and strong ((b) and (d)) stiffening effects. Consistent with the observations in Fig. 14, complete BGs shift down towards lower frequencies. Moreover, the position of complete BGs is highly tunable via deformation. In particular, in the undeformed laminate with $v_a = 0.95$, $\mu_a/\mu_b = 100$, $\Lambda_a/\mu_a = 10$, and $\Lambda_b/\mu_b = 5$, the lowest complete BG has the width $\Delta f_n = 0.29$ with the lower boundary at $f_n = 0.92$, while for the laminate under in-plane compression, $\lambda = 0.5$, the lowest complete BG has the width $\Delta f_n = 0.63$ with the lower boundary at $f_n = 0.57$ (see Fig. 15(a)). In case of the equibiaxial compression, $\lambda = 0.5$, the lowest complete BG has the width $\Delta f_n = 0.75$ with the lower boundary at $f_n = 0.46$ (see Fig. 15(c)). Consequently, the equibiaxial deformation has a more pronounced influence on the position of complete BGs as compared to the effect of the in-plane deformation.

A comparison of Fig. 15(a) and (b) (and also Fig. 15(c) and (d)) shows that in the laminate with Gent phases the PBGs are wider and they appear at higher frequencies compared to the PBGs in the laminates with neo-Hookean phases. This leads to the shifting of complete BGs towards higher frequencies. In particular, the lower boundary of the first complete BG in the laminate undergoing the in-plane contraction of the magnitude $\lambda = 0.5$ shifts from $f_n = 0.57$ up to $f_n = 0.71$ (compare Fig. 15(a) and (b)). In the case of the equibiaxial contraction of magnitude $\lambda = 0.7$, the lower boundary of the first complete BG shifts from $f_n = 0.57$ up to $f_n = 0.69$ (compare Fig. 15(c) and (d)). Similarly to the laminates considered in Fig. 12, the transformations of the BGs correlate with the changes in the thicknesses of the layers and phase velocities within each layer. In particular, an increase in the thicknesses of the layers ($d/d^o > 1$) shifts BGs towards lower frequencies whereas a decrease in the layer thicknesses ($d/d^o < 1$) shifts BGs towards higher frequencies. Once again, an increase in phase velocities ($c/c^o > 1$) shifts BGs towards higher frequencies, and a decrease in phase velocities ($c/c^o < 1$) shifts BGs towards lower frequencies.

3.2.3. An example of band gap structures for possible realistic layered materials

In this section, we provide a calculation of the BG structure for composites made of silicon rubber (Elite Double 32, Zhermarck) and one of a digital material used in multimaterial 3D printing (A85). Both of these materials can be described by the extended neo-Hookean strain energy function (30). Table 1 summarizes the corresponding parameters for these deformable materials. The phase a is made of the digital material A85, and the phase b is made of the silicon rubber Zhermarck Elite Double 32. Fig. 16 shows pressure and shear wave BGs as functions of the volume fraction of phase a in the undeformed and deformed laminates. We observe that the lowest complete BG has a maximal width for a certain volume fraction v_a in the undeformed laminate. In particular, for the laminate with $v_a = 0.87$ the lowest complete BG has width $\Delta f_n = 0.26$ with the lower boundary at $f_n = 2.50$, while for the laminate with $v_a = 0.1$ the lowest complete BG has width $\Delta f_n = 0.3$ with the lower boundary at $f_n = 3.4$. Consistent with previous observations in this paper, an extension of the laminate does not change the position of SBGs and shifts up PBGs towards higher frequencies. For example, the in-plane extension of the magnitude $\lambda = 1.3$ shifts the lower boundary of the first PBG from $f_n = 2.50$ up to $f_n = 3.23$ in the laminate with $v_a = 0.87$ (compare Fig. 16(a) and (b)).

To clarify how the pressure wave and complete BGs depend on deformation in the laminates made of silicon rubber (Elite Double

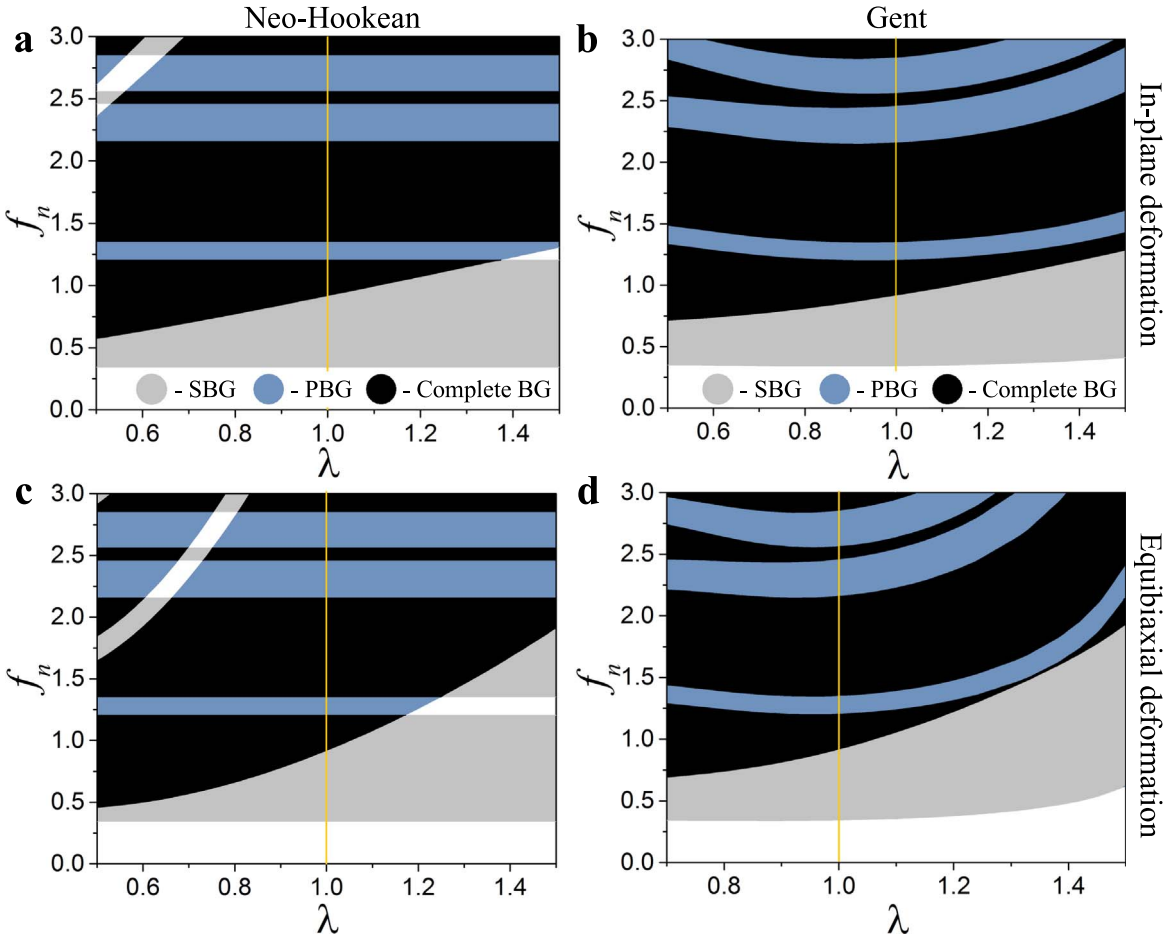

Fig. 15. Band gaps vs. stretch ratio for laminates subjected to ((a) and (b)) in-plane tension and ((c) and (d)) equibiaxial deformations. $\nu_a = 0.95$, $\mu_a/\mu_b = 100$, $\Lambda_a/\mu_a = 10$, $\Lambda_b/\mu_b = 5$, $\rho_{0a}/\rho_{0b} = 1$, and $J_{ma} = J_{mb} = 2.5$. (a) and (c) refer to laminate with neo-Hookean phases and (b) and (d) refer to laminate with Gent phases.

32, Zhermarck) and the digital material (A85), we present BGs as functions of the applied stretch ratio in Fig. 17. Fig. 17(a) and (b) illustrate how the in-plane (27) and equibiaxial deformations (28) of the layered material with $\nu_a = 0.3$ influence the BG structure. We observe that PBGs narrow and shift towards lower frequencies in the laminate undergoing contraction while an extension of the laminate widens and shifts PBGs towards higher frequencies. In particular, the lower boundary of the first PBG shifts from $f_n = 3.05$ down to $f_n = 2.45$ and its width decreases from $\Delta f_n = 1.33$ down to $\Delta f_n = 1.07$ in the laminate subjected to the in-plane contraction of the magnitude $\lambda = 0.8$ (see Fig. 17(a)). The equibiaxial deformation has a more pronounced effect on the PBGs; in particular, the equibiaxial contraction of the magnitude $\lambda = 0.8$ shifts the lower boundary of the first PBG from $f_n = 3.05$ down to $f_n = 1.98$ and narrows it from $\Delta f_n = 1.33$ down to $\Delta f_n = 0.86$ (see Fig. 17(b)). Remarkably, complete BGs can be induced in a required frequency range by deformation while the undeformed laminate does not produce complete BGs in that range. For example, the considered here laminate has no complete BGs (in the frequency range up to $f_n = 3$) in the undeformed state while it has the complete BG of width $\Delta f_n = 0.49$ when subjected to the in-plane contraction of the stretch ratio magnitude $\lambda = 0.83$ (see Fig. 17(a)).

Fig. 17 also shows the Bragg limit frequency, $f^{(BL)} = \overline{c}_{pw}/(2\pi d)$, and an estimate for the resonance frequency of stiffer layer, $f^{(R)} = \overline{c}_{pw}/(2\pi d_a)$. Clearly, the first complete BG occurs in the vicinity of the resonance frequency of the stiffer layer; moreover, it occurs above the Bragg limit. Hence, a composition of both Bragg scattering and inner resonance of stiffer layers participate in formation of complete BGs. In other words, in layered media the mechanism forming complete BGs is based on the destructive

Table 1
Material parameters.

Material	μ, MPa	Λ, MPa	ρ_0, kg/m^3
Elite Double 32	0.444	22.2	1050
Digital material (A85)	22	1100	1200

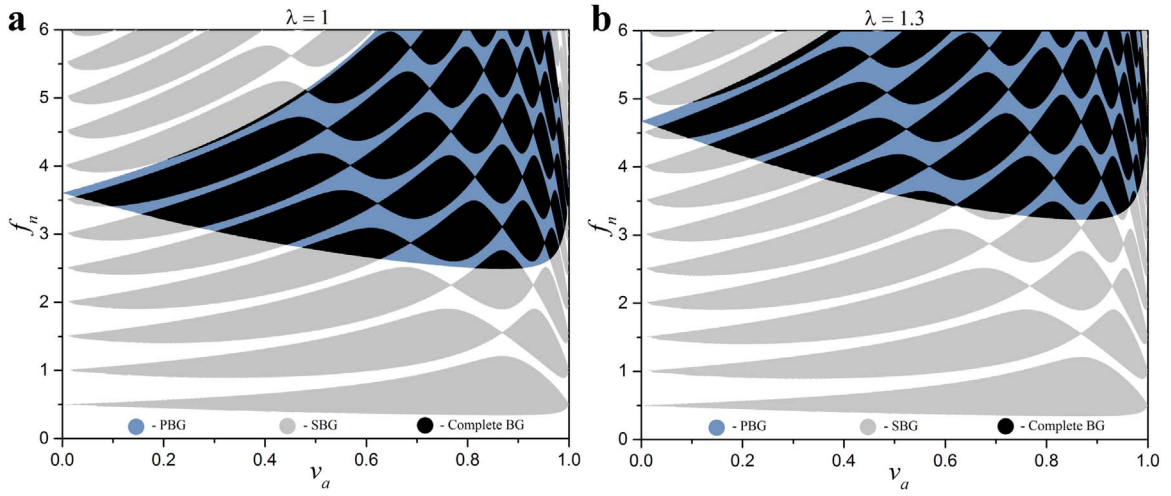

Fig. 16. Band gaps vs. volume fraction of the phase a in (a) the undeformed laminate and (b) the one subjected to the in-plane tension of the magnitude $\lambda = 1.3$ with $\mu_a/\mu_b = 50$, $\Lambda_a/\mu_a = 50$, $\Lambda_b/\mu_b = 50$, and $\rho_{0a}/\rho_{0b} = 1.14$. The gray, blue, and black colors correspond to the shear wave, pressure wave, and complete BGs, respectively. (For interpretation of the references to color in this figure caption, the reader is referred to the web version of this paper.)

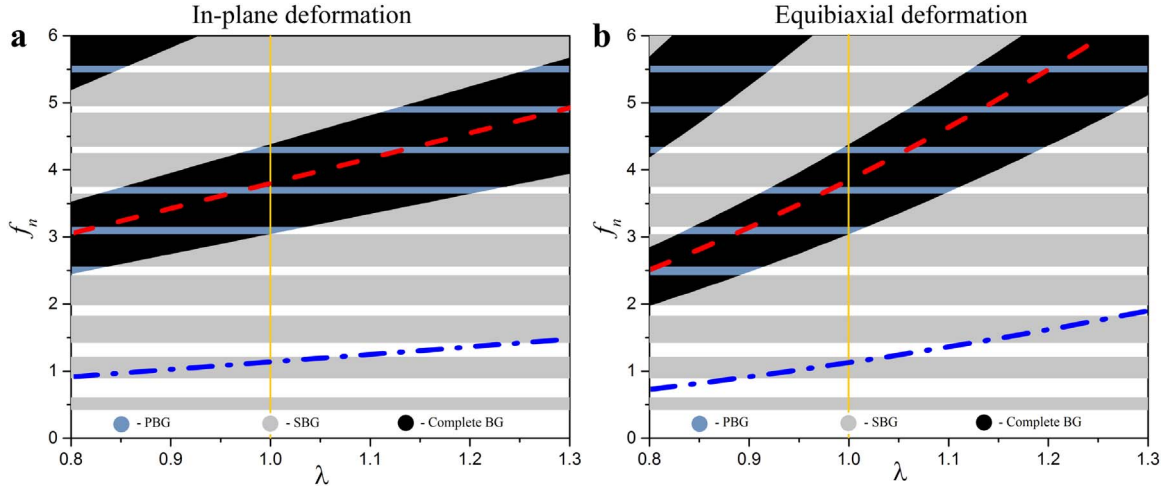

Fig. 17. Band gaps vs. in-plane (a) and equibiaxial (b) deformations for the laminate with $\nu_a = 0.3$, $\mu_a/\mu_b = 50$, $\Lambda_a/\mu_a = 50$, $\Lambda_b/\mu_b = 50$, and $\rho_{0a}/\rho_{0b} = 1.14$. The blue dash-dotted and red dashed curves correspond to estimates of the Bragg limit and the resonance frequency of stiffer layer, respectively. (For interpretation of the references to color in this figure caption, the reader is referred to the web version of this paper.)

interference of the scattered waves by the stiffer layers and inner resonances of these layers.

4. Conclusions

We considered elastic wave propagation in soft periodic layered media undergoing finite deformations. Firstly, based on an exact analytical solution for finitely deformed laminates with alternating neo-Hookean phases, we derived explicit relations for phase (41) and group velocities (55) and (56). Secondly, we obtained long wave estimates (59) and (63) for the phase velocities of pressure and shear waves propagating perpendicular to the layers in the finitely deformed *compressible* laminates with neo-Hookean and Gent phases. These estimates provide the important information on elastic wave propagation with wavelengths larger than microstructure size, namely $l \gtrsim \pi d$; moreover, these explicit expressions may provide estimates for transversely isotropic fiber composites. Thirdly, we provided a detailed analysis of the band gap structures for the waves propagating perpendicular to the layers in the incompressible and compressible layered materials. Specifically, we identified the key parameters and mechanisms influencing the shear wave, pressure wave, and complete BGs. Based on the analysis, we revealed the advantageous compositions of the laminates producing the wide BGs in the low-frequency range.

For *incompressible* laminates, we showed that (i) a small amount of a soft phase in a stiffer matrix produces wide SBGs; (ii) SBG structure in layered materials with phases exhibiting weak stiffening effects is not influenced by deformation because deformation induced changes in geometry and effective material properties compensate each other; (iii) contraction or extension of the laminate

with stiffening in phases widens and shifts up SBGs towards higher frequencies due to the stronger effect of deformation induced changes in the material properties (as compared to the geometry changes).

For *compressible* laminates, we showed that (i) wide complete BGs can be produced by composing periodic laminates with thin highly compressible layers embedded in a nearly incompressible matrix; (ii) the dominant mechanism influencing PBGs is the deformation induced change in the thicknesses of the layers; (iii) by application of deformation to the laminates with highly compressible phases, complete BGs in the low-frequency range can be produced. These low-frequency range BGs are not accessible for laminates with nearly incompressible phases.

In this work, we considered small amplitude motions (superimposed on finite deformations); therefore, the presented results cannot be fully applied for finite amplitude elastic waves propagating in soft microstructured materials. This can be potentially an interesting direction of future research. Another aspect is the influence of the direction of elastic wave propagation. We fully address this aspect in the analysis of long waves considering any direction of wave propagation and any applied deformations. However, our analysis of elastic wave band gaps focuses on the normal direction of wave propagation, and the consideration of oblique elastic waves would require different techniques such as Bloch–Floquet numerical analysis or transfer matrix methods. Finally, we note that a consideration of dissipation can potentially improve the accuracy of the predictions, especially for the composites with constituents characterized by strong damping effects (Babaee et al., 2015).

Acknowledgments

This work was supported by the BASF North American Center for Research of Advanced Materials. S.R. and P.G. gratefully acknowledge the support of the Israel Science Foundation (grant 1550/15 and 1973/15). S.R. thanks the support of Taub Foundation through the Horev Fellowship – Leaders in Science and Technology.

References

Arruda, E.M., Boyce, M.C., 1993. A three-dimensional constitutive model for the large stretch behavior of rubber elastic materials. J. Mech. Phys. Solids 41, 389–412.
Auld, B., 1990. Acoustic Fields and Waves in Solids. Krieger Publishing Company, Malabar, Fl.
Auriault, J.-L., 1994. Acoustics of heterogeneous media: macroscopic behavior by homogenization. Curr. Top. Acoust. Res. 1, 63–90.
Auriault, J.-L., Bonnet, G., 1985. Dynamique des composites lastiques priodiques. Arch Mech. 37 (4–5), 269–284.
Auriault, J.-L., Boutin, C., 2012. Long wavelength inner-resonance cut-off frequencies in elastic composite materials. Int. J. Solids Struct. 49, 3269–3281.
Babaee, S., Shim, J., Weaver, J., Chen, E., Patel, N., Bertoldi, K., 2013. 3D soft metamaterials with negative Poisson's ratio. Adv. Mater. 25 (36), 5044–5049.
Babaee, S., Viard, N., Wang, P., Fang, N.X., Bertoldi, K., 2016. Harnessing deformation to switch on and off the propagation of sound. Adv. Mater. 28 (8), 1631–1635.
Babaee, S., Wang, P., Bertoldi, K., 2015. Three-dimensional adaptive soft phononic crystals. J. Appl. Phys. 117, 244903.
Bedford, A., Drumheller, D., 1994. Elastic Wave Propagation. Wiley, Bedford.
Bertoldi, K., Boyce, M.C., 2008a. Mechanically triggered transformations of phononic band gaps in periodic elastomeric structures. Phys. Rev. B 77 (5), 052105.
Bertoldi, K., Boyce, M.C., 2008b. Wave propagation and instabilities in monolithic and periodically structured elastomeric materials undergoing large deformations. Phys. Rev. B 78, 184107.
Bertoldi, K., Boyce, M.C., Deschanel, S., Prange, S.M., Mullin, T., 2008. Mechanics of deformation-triggered pattern transformations and superelastic behavior in periodic elastomeric structures. J. Mech. Phys. Solids 56 (8), 2642–2668.
Boulanger, P., Hayes, M., Trimarco, C., 1994. Finite-amplitude plane waves in deformed Hadamard elastic materials. Geophys. J. Int. 118 (2), 447–458.
Brunet, T., Leng, J., Mondain-Monval, O., 2013. Soft acoustic metamaterials. Science 342 (6156), 323–324.
Crosby, A.J., 2010. Why should we care about buckling? Soft Matter 6, 5660.
deBotton, G., 2005. Transversely isotropic sequentially laminated composites in finite elasticity. J. Mech. Phys. Solids 53, 1334–1361.
Destrade, M., Ogden, R.W., 2011. On magneto-acoustic waves in finitely deformed elastic solids. Math. Mech. Solids 16, 594–604.
Galich, P.I., Rudykh, S., 2015a. Comment on Disentangling longitudinal and shear elastic waves by neo-Hookean soft devices [Appl. Phys. Lett. 106 (2015) 161903]. Appl. Phys. Lett. 107, 056101., http://dx.doi.org/10.1063/1.4928392.
Galich, P.I., Rudykh, S., 2015b. Influence of stiffening on elastic wave propagation in extremely deformed soft matter: from nearly incompressible to auxetic materials. Extreme Mech. Lett. 4, 156–161.
Galich, P.I., Rudykh, S., 2016. Manipulating pressure and shear elastic waves in dielectric elastomers via external electric stimuli. Int. J. Solids Struct. 91, 18–25.
Gei, M., Roccabianca, S., Bacca, M., 2011. Controlling bandgap in electroactive polymer-based structures. IEEE/ASME Trans. Mechatron. 16 (1), 102–107.
Gent, A.N., 1996. A new constitutive relation for rubber. Rubber Chem. Technol. 69, 59–61.
Horgan, C.O., Saccomandi, G., 2004. Compressible hyperelastic isotropic materials, constitutive models, limiting chain extensibility. J. Elast. 77 (2), 123–138.
Hussein, M.I., 2009. Reduced Bloch mode expansion for periodic media band structure calculations. Proc. R. Soc. Lond. Ser. A 465 (2109), 2825–2848.
Khelif, A., Adibi, A., 2016. Phononic Crystals. Springer, New York.
Kittel, C., 2004. Introduction to Solid State Physics 8th ed.. Wiley, Hoboken, N.J.
Kolle, M., Lethbridge, A., Kreysing, M., Baumberg, J., Aizenberg, J., Vukusic, P., 2013. Bio-inspired band-gap tunable elastic optical multilayer fibers. Adv. Mater. 25 (15), 2239–2245.
Kushwaha, M., Halevi, P., Dobrzynski, L., Djafari-Rouhani, B., 1993. Acoustic band structure of periodic elastic composites. Phys. Rev. Lett. 71 (13), 2022–2025.
Kushwaha, M., Halevi, P., Martinez, G., Dobrzynski, L., Djafari-Rouhani, B., 1994. Theory of acoustic band structure of periodic elastic composites. Phys. Rev. B 49 (4), 2313–2322.
Li, Y., Kaynia, N., Rudykh, S., Boyce, M.C., 2013. Wrinkling of interfacial layers in stratified composites. Adv. Eng. Mater. 15 (10), 921–926.
Liu, X.N., Hu, G.K., Huang, G.L., Sun, C.T., 2011. An elastic metamaterial with simultaneously negative mass density and bulk modulus. Appl. Phys. Lett. 98, 251907.
Liu, Z., Zhang, X., Mao, Y., Zhu, Y., Yang, Z., Chan, C., Sheng, P., 2000. Locally resonant sonic materials. Science 289 (5485), 1734–1736.
Mousanezhad, D., Babaee, S., Ghosh, R., Mahdi, E., Bertoldi, K., Vaziri, A., 2015. Honeycomb phononic crystals with self-similar hierarchy. Phys. Rev. B 92, 104304.
Nayfeh, A.H., 1995. Wave Propagation in Layered Anisotropic Media: With Applications to Composites. Elsevier Science, Amsterdam, New York.
Ogden, R.W., 1997. Non-Linear Elastic Deformations. Dover Publications, New York.
Rosen, B.W., 1965. Mechanics of composite strengthening. In: Fibre Composite Materials. American Society for Metals, Ohio, pp. 37–75.
Rudykh, S., Boyce, M., 2014a. Analysis of elasmoid fish imbricated layered scale-tissue systems and their bio-inspired analogues at finite strains and bending. IMA J. Appl. Math. 79, 830–847.
Rudykh, S., Boyce, M., 2014b. Transforming wave propagation in layered media via instability-induced interfacial wrinkling. Phys. Rev. Lett. 112, 034301.
Rudykh, S., deBotton, G., 2012. Instabilities of hyperelastic fiber composites: micromechanical versus numerical analyses. J. Elast. 106, 123–147.
Rudykh, S., Ortiz, C., Boyce, M., 2015. Flexibility and protection by design: imbricated hybrid microstructures of bio-inspired armor. Soft Matter 11, 2547–2554.
Rytov, S., 1956. Acoustical properties of a thinly laminated medium. Sov. Phys. Acoust. 2, 68–80.

Slesarenko, V., Rudykh, S., 2016. Harnessing viscoelasticity and instabilities for tuning wavy patterns in soft layered composites. Soft Matter 12, 3677–3682.
Spinelli, S.A., Lopez-Pamies, O., 2015. Some simple explicit results for the elastic dielectric properties and stability of layered composites. Int. J. Eng. Sci. 88, 15–28.
Tanaka, Y., Tomoyasu, Y., Tamura, S.-I., 2000. Band structure of acoustic waves in phononic lattices: two-dimensional composites with large acoustic mismatch. Phys. Rev. B 62 (11), 7387–7392.
Triantafyllidis, N., Maker, B.N., 1985. On the comparison between microscopic and macroscopic instability mechanisms in a class of fiber-reinforced composites. J. Appl. Mech. Trans. ASME 52, 794–800.
Tzianetopoulou, T., 2007. Micro-and Macromechanics of Single Crystal and Polygrannular Lamellar Block Copolymers (Ph.D. thesis). MIT.
Wang, P., Shim, J., Bertoldi, K., 2013. Effects of geometric and material non-linearities on the tunable response of phononic crystals. Phys. Rev. B 88, 014304.
Zhou, X.-Z., Wang, Y.-S., Zhang, C., 2009. Effects of material parameters on elastic band gaps of two-dimensional solid phononic crystals. J. Appl. Phys. 106, 1.